

Comparing erosion and rill development processes by simulated upslope inflow in two red soils from subtropical China

Pei Tian^a, Yuwei Gong^a, Fanghua Hao^a, Lin Chen^b, Yang Yang^c, Wenzhao Guo^{d,*}, Huaqing Wu^a, Wenjie Zhang^a

^a Key Laboratory for Geographical Process Analysis & Simulation of Hubei Province, Central China Normal University, Wuhan 430079, PR China

^b Department of Environmental Sciences, University of California Riverside, Riverside, CA 92521, USA

^c Sameng Inc., 17205-106A Ave Edmonton, Alberta, Canada

^d State Key Laboratory of Soil Erosion and Dryland Farming on the Loess Plateau, Institute of Water and Soil Conservation, Northwest A&F University, Yangling 712100, Shaanxi, PR China

ARTICLE INFO

Keywords:

Inflow rate
Rill erosion
Rill morphology
Sediment size distribution
Flow hydrodynamics

ABSTRACT

Rill erosion is an important component of soil erosion, however, the process and mechanism of rill erosion on red soil slopes are not clear enough. In this paper, runoff scouring experiments were conducted with five varying inflow rates ($8.5, 10, 11.5, 13, 14.5 \text{ L min}^{-1} \text{ m}^{-1}$) and one slope (8°) using two typical red soils in subtropical China: Ultisols derived from shale (*UDS*) and Ultisols derived from quaternary red clay (*UDQ*). The results showed that for the two red soils, runoff rate, sediment yield rate, and rill erosion amount were all positively correlated with inflow rates in linear relationships ($p < 0.05$). The high sand and low clay contents in eroded sediments were closely related to the original soil texture (dominated by clay and silt) and rill flow energy. Stream power and unit stream power were the optimal hydraulic parameters to characterize rill erosion mechanisms for *UDS* and *UDQ*, respectively. For *UDQ* with higher clay content and bulk density, the sediment yield process was more stable and the sand content in the eroded sediments was significantly higher than that of *UDS*, while the silt content was significantly lower. The rill flow of *UDQ* had slower velocity and larger Darcy–Weisbach resistance coefficient than that of *UDS*. For *UDS* with lower clay and higher sand content, the average sediment yield rate and rill depth were 2.26–4.71 and 2.79–6.53 times of *UDQ*, respectively, and the rill erodibility parameter was 1.84 times that of *UDQ*. The results are helpful for understanding the rill erosion mechanism and preventing soil loss in subtropical areas.

1. Introduction

Ultisols are widespread in southern China, American south, south-east Asia and some other subtropical and tropical regions (Wang et al., 2012). The red soils in subtropical China, classified as Ultisols using the U.S. Soil Taxonomy System, occupy approximately 1.14 million km² (Shi et al., 2010), and are highly weathered and particularly susceptible to severe soil erosion (Zhang et al., 1996; Peng et al., 2016). Due to the undulating topography, poor soil properties, improper land use and soil management, the area affected by water erosion accounts for 25% of

total land areas in the red soil region of subtropical China (Zhang et al., 2004; Yu et al., 2006; Fang et al., 2017).

As an important component of soil erosion on cultivated slopes, rill erosion is an intermediate process between sheet and gully erosions (Miao et al., 2010; Kou et al., 2021). Eroding rills are important sediment sources and primary channels for sediment transportation on hillslopes (Wirtz et al., 2012; Vinci et al., 2015; Di Stefano et al., 2021), for the concentrated flow in rills has higher hydraulic erosive force and transport capacity than the sheet flow (Wirtz et al., 2013). Due to the severe soil erosion, rills and gullies caused by washing of abundant

Abbreviations: *UDQ*, Ultisols derived from quaternary red clay; *UDS*, Ultisols derived from shale; *PSD*, particle size distribution; *RR*, mean runoff rate during the sampling period $\text{L min}^{-1} \text{ m}^{-2}$; *SYR*, mean sediment yield rate during the sampling period $\text{g m}^{-2} \text{ min}^{-1}$; *V*, the average flow velocity in rill cross section m s^{-1} ; *h*, The average runoff depth *m*; *Re*, the Reynolds number; *Fr*, the Froude number; *f*, the Darcy–Weisbach resistance coefficient; *n*, the Manning roughness coefficient; *τ*, the flow shear stress N m^{-2} ; *ω*, the stream power of slope flow $\text{N m}^{-1} \text{ s}^{-1}$; *φ*, the unit stream power m s^{-1} ; *RER*, rill erosion rate $\text{g m}^{-2} \text{ s}^{-1}$.

* Corresponding author.

E-mail addresses: tianpei@ccnu.edu.cn (P. Tian), wenzhaoguo@nwafu.edu.cn (W. Guo).

rainfall-runoff are obvious on soil surfaces in this region (Zhang et al., 2004; Wang et al., 2012). However, previous studies related to Ultisols erosion mainly focused on sheet erosion (Zhao et al., 2015; Wu et al., 2018), interrill erosion (Yan et al., 2008, Yan et al., 2010; Wu et al., 2017), gully erosion (Luffman et al., 2015; Brecheisen and Richter, 2021) and aggregate stability (Chappell et al., 1999; Wang et al., 2016; Xiao et al., 2017; da Silva et al., 2020; Wu et al., 2021). And the mechanism of rill erosion on red soil slopes is still not clear. A thorough understanding of rill erosion mechanisms on red soil slopes is helpful for carrying out targeted soil loss control management, which is practically significant for maintaining ecological security and socioeconomic sustainability in Ultisols areas.

Rill development is the process of soil detachment and sediment transport by concentrated surface flow (Kimaro et al., 2008). Rill erosion occurs when flow erosivity exceeds a certain threshold of soil resistance (Govers et al., 2007; Knapen et al., 2007), so rill development is largely affected by flow erosivity and soil anti-erodibility. The flow erosivity is closely related to upslope inflow rate (Berger et al., 2010), and Zhang et al. (2003) found soil detachment rates more sensitive to upslope inflow discharge than slope gradients. The erosivity of slope runoff can be described by the hydraulic parameters such as flow pattern (Foster et al., 1984), flow velocity (Govers et al., 2007), flow shear stress (Nearing et al., 1989; Giménez and Govers, 2002), stream power (Nearing et al., 1999; Berger et al., 2010) and unit stream power (Morgan et al., 1998). The analysis of slope flow hydraulic characteristics and their variations are critical to understanding the dynamic mechanism of hillslope soil erosion process. In China, the studies researching the hydrodynamic mechanisms of rill erosion were primarily aiming at loessial hillslopes (Peng et al., 2015; Zhang et al., 2015; Shen et al., 2016; Niu et al., 2020; Tian et al., 2017, Tian et al., 2020). And limited research deeply investigated the hydrodynamic mechanisms of rill erosion on red soil slopes, and the anti-erodibility to water flow of different red soils remains ambiguous.

Soil property is an intrinsic factor influencing soil anti-erodibility (Assouline and Ben-Hur, 2006), and can reflect the possibility of rill erosion on red soils (Cai et al., 2004). According to Wu et al. (2017), soil properties (mainly clay content) had great impacts on the erosion process and sediment yield for Ultisols derived from quaternary red clay. And soil aggregation characteristics is a suitable indicator for the rill erosion sensitivity of red soil in subtropical China (Shi et al., 2010). While the main physical and chemical properties of soil were largely determined by parent material (Muhs et al., 2001; Rawlins et al., 2003), so as the differences of soil erosion processes and rates (Rodrigo-Comino et al., 2018). Therefore, to clarify the rill mechanisms from the perspective of soil properties, study aiming at red soils derived from different parent materials is needed. However, to our knowledge, limited attempts have been made to systematically investigate the hydrological and sedimentological processes of rill erosion for red soils derived from different parent materials.

Rill morphology plays a significant role in determining surface runoff and soil loss from hillslopes (Govindaraju and Kavvas, 1994), because it changes the flow characteristics and underlying surface conditions (Zhang et al., 2016; Wu et al., 2018). The rill flows, with higher depth and velocity, can transport more sediment downslope than the overland flows (Gatto, 2000). Di Stefano et al. (2013) obtained the empirical relationship among the length, width, depth and volume of rills through field investigation, and found the above morphological parameters were the main indexes affecting the sediment yield in the rill-interrill erosion system on slope. The variation of rill width and depth can reflect the variation of rill development and rill flow energy (Mancilla et al., 2005), and the width-depth ratio can reflect the shape of rill cross section objectively (He et al., 2016). Many studies have investigated rill network development and the temporal-spatial variations in rill cross-section morphology (Brunton and Bryan 2000; Rejman and Brodowski 2005; Bruno et al. 2008; Shen et al., 2015; Wang et al., 2019; Jafarpoor et al., 2022). Comparative analysis for rill morphology between different loess

soils was conducted by Fang et al. (2015), while studies comparing rill development for red soils with different textures are still lacking.

The sediment particle size distribution (PSD) can well reflect the erosion process, and has an important influence on sediment transportation and deposition (Wang et al., 2014). PSD depends on soil properties, rainfall-runoff characteristics, surface conditions, and vegetation coverage (Shi et al., 2012; Ding and Huang, 2017; Saygin and Erpul, 2019). Wu et al. (2018) observed that the sediment size increased with rainfall intensity and clay content. Shi et al. (2013) indicated that most of the clay was eroded in the form of aggregates and sand-sized particles were predominantly aggregates of finer particles. Sediment sorting and transport mechanisms by concentrated flow which were closely related to flow hydrodynamics and soil properties (Asadi et al., 2011), varied in different rill erosion stages. The general agreement is that interrill erosion results in selective removal of fine particles, whereas rill erosion is less selective (or nonselective) after a specific critical flow shear stress is exceeded (Durnford and King, 1993; Malam Issa et al., 2006; Hao et al., 2019). Sediment sorting and its dynamics reveal the behavior and interaction of different components, which facilitate the understanding of detachment, transport and sedimentation processes (Defersha and Melesse, 2012; Wu et al., 2017).

Therefore, in this study, a comparative analysis was conducted to investigate erosion and rill development processes of two red soils derived from typical parent materials (argillaceous shale and quaternary red clay) in subtropical China. A series of indoor runoff scouring experiments under the combinations of five inflow rates and two red soils were carried out to achieve the three objectives: (1) to investigate and compare the rill erosion, sediment particle size distribution, flow hydraulics and rill morphology of the two red soils; (2) to discuss the impacts of inflow rates and soil texture on erosion and rill development processes; (3) to clarify the sediment sorting and hydrodynamic mechanisms of rill erosion, as well as the differences in these mechanisms of the two red soils.

2. Materials and methods

2.1. The study sites and experimental materials

Two representative sites with red soils were selected in Heshengqiao Town ($114^{\circ}06' \text{--} 114^{\circ}43'E$, $29^{\circ}39' \text{--} 30^{\circ}02'N$) and Dafan Town ($114^{\circ}14' \text{--} 114^{\circ}58'E$, $29^{\circ}40' \text{--} 30^{\circ}03'N$), Xianning City, Hubei Province, China (Fig. 1). The study sites, located in the hilly area of southeastern Hubei Province, have a subtropical humid continental monsoon climate with an average annual precipitation and temperature of 1300 mm and 16.8°C , respectively. Low mountains and hills with slope grades below 25° are the main forms of landform in this area (Tian et al., 2021).

The two red soils derived from different parent materials are widely distributed in this region. According to the U.S. Soil Taxonomy, the two red soils are classified as Ultisols, which are Ultisols derived from shale (*UDS*) and Ultisols derived from quaternary red clay (*UDQ*). The basic properties of the tested soils are shown in Table 1. Among them, the clay content of *UDQ* is higher than that of *UDS*, while the sand content is the opposite. Meanwhile, the silt contents have little difference between them.

The experiments were completed in the Key Laboratory of Geographic Process Analysis & Simulation of Wuhan, Hubei Province, China. The experimental facility was composed of three independent parts (Fig. 2): (i) Test soil flume, the main body is two parallel flumes with a size of 1.5-m length, 0.25-m width and 0.3-m depth, with holes (2 cm aperture) evenly distributed at the bottom to facilitate drainage. The side wall and bottom surface were smooth, and the bottom of the flume was supported by a steel frame. The slope can be adjusted in the range of 0 to 20° by pulling lifting device with a pulley. (ii) Steady flow flume, which was located in front of the test soil flume and separated by a stainless steel plate. After the discharge reached a predetermined value, the water first flowed through the steady flow flume to ensure that it

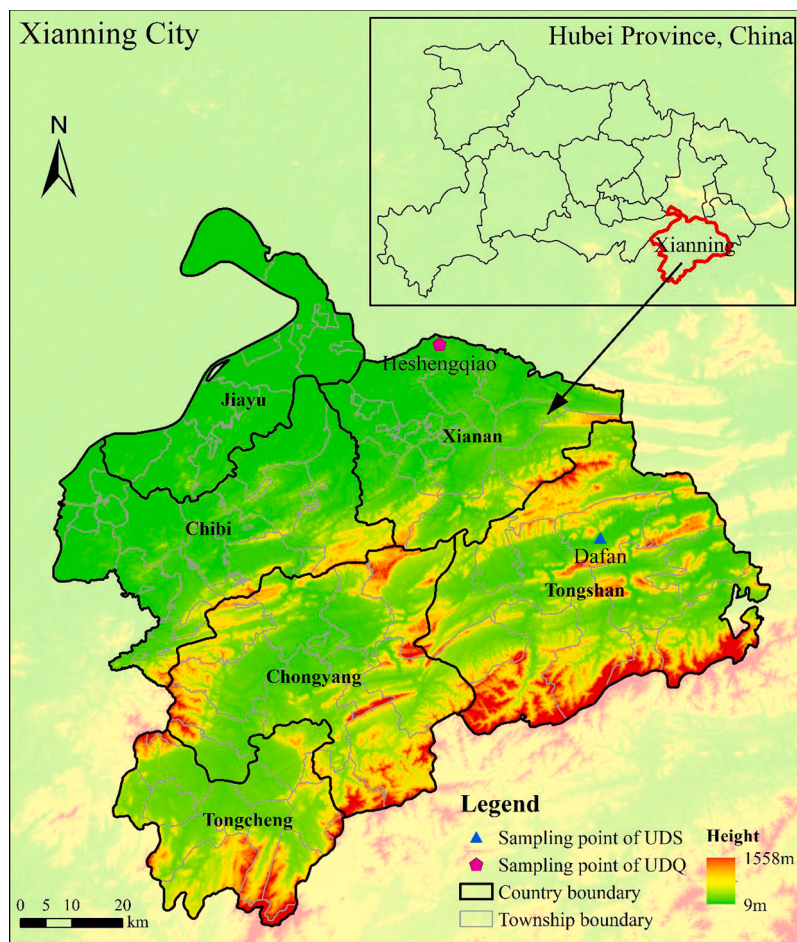


Fig. 1. The soil sampling point location.

Table 1
Basic properties of the tested soils.

Sampling site	Latitude and longitude	Soil type	Land surface conditions	Soil texture	Bulk density (g cm ⁻³)	Particle composition (100%)
						Clay Silt Sand
Dafan Town	29°38'N, 114°34'E	UDS	Forest-arable transition zone	Silty clay loam	1.081	23. 53 56. 77 19. 70
Heshengqiao Town	30°1'N, 114°21'E	UDQ	Woodland	Silty clay	1.32	35. 07 60. 52 4. 41

UDS: Ultisols derived from shale; UDQ: Ultisols derived from quaternary red clay. Clay: <0.002 mm; Silt: 0.002–0.05 mm; Sand: 0.05–2 mm.

uniformly and smoothly flowed into the test soil flume. (iii) Water supply device, including water supply source and peristaltic pump. The water supply source was tap water, while the peristaltic pump was used to control discharges accurately.

2.2. Experimental design and procedures

Five inflow rates (8.5, 10, 11.5, 13 and 14.5 L min⁻¹ m⁻¹), two red soils (UDS and UDQ) and one slope gradient (8°) were employed in this experiment. There were 10 experimental treatments in its totality, and each treatment was repeated twice. The inflow rates were determined according to the range of rainfall intensities and inflow rates designed in the previous studies on red soil slopes (Guo et al., 2018; Wu et al., 2018; Hao et al., 2019), and combining with the size of the test soil flume. The slope of 8° was chosen to characterize the common slope in the study area, where the lands with slopes between 5° and 15° are widely used for farming (Guo et al., 2018).

During sampling in the field, the leaf litter layer at the sampling point

was removed, and the upper soil layer (0–20 cm) was taken. Then soil samples were brought back to the laboratory for air-drying, grinding and passing through a 2 mm sieve to remove roots, rocks and other debris. Before filling the test soil flume with soil samples, the drying method was used to measure the moisture content of the test soil to determine the required fill weight. The soil bulk densities were controlled at 1.1 g cm⁻³ and 1.3 g cm⁻³ for the UDS and UDQ samples, respectively. Firstly, a 5-cm sand layer was packed at the bottom of the test soil flume and covered with geotextile material to ensure fine permeability. After that, a 15-cm air-dried soil layer was packed and compacted at a 5-cm interval on top of the sand layer. After the lower soil layer was packed, the surface was slightly raked to prevent delamination, and the upper soil layer was added subsequently. Meanwhile, the soil on the side wall of the test soil flume should be compacted as much as possible to minimize the influence of boundary effect. After the above procedures, the surface of test soil was covered with geotextile material and uniformly sprinkled to prewet. Runoff scouring experiments were conducted after the soil was allowed to stand for 24 h. Prior to running experiments, the inflow



Fig. 2. Schematic diagram of experimental device.

rate was calibrated by peristaltic pump. During Runoff scouring, the initiation time of runoff was recorded. Each experiment lasted for 30 min in a windless indoor environment. Runoff and sediment samples were collected at the 1-min interval.

The volumes of these samples were measured with a measuring cylinder and then dried them in an oven at 105 °C to obtain the sediment yield. Additionally, the PSD of collected sediment samples were measured with a Mastersizer 3000 laser particle analyzer (Malvern Instruments, Malvern, UK). During each experimental running, flow velocities of the upper slope (0–50 cm), middle slope (50–100 cm), and lower slope (100–150 cm) were measured with a dye tracer (KMnO_4) method. After rills occurred, the dye tracer was instilled into rills to measure rill flow velocity. The flumes were marked at 50 cm and 100 cm to assist the measurements, and the tracer movement time at the marked

distance (0.5 m) was determined based on the color-front propagation using a stop-watch. In addition, to avoid the disturbance of the dye flowing downslope, the measuring sequence was lower, middle and upper slope, respectively. Also, the width of water-crossing section in rills at the three slope sections was measured using a vernier caliper. The slope was photographed at the 5-min interval to observe the changes of the water flow and the shape of the rill during each experiment. After completing each runoff scouring, rill width and depth measurements were conducted at 6 cross-sections uniformly distributed along each rill channel from top to bottom. And the rill volumes were calculated according to the measured morphology data, which in turn, to estimate the rill erosion magnitude combined with the bulk densities of soil samples.

2.3. Data calculation and analysis

2.3.1. Runoff and sediment yield rate

$$RR = (M - m) / (\rho t A) \quad (1)$$

$$SYR = m / (At) \quad (2)$$

where t is the sampling time for a runoff sample (min); RR is the mean runoff rate at the flume outlet during the sampling period t ($\text{L min}^{-1} \text{m}^{-2}$); SYR is the mean sediment yield rate at the flume outlet during the sampling period t ($\text{g m}^{-2} \text{min}^{-1}$); M is the total mass of a runoff sample, g; m is the mass of dry sediment of a runoff sample (g); ρ is the density of water (g cm^{-3}); A is the surface area of the flume (m^2).

2.3.2. Sediment particle size distribution

As the effective particle size of sediments probably better indicate how the soil was detached and transported by raindrop and runoff especially for soils in strong aggregation compared to the ultimate particle size (Shi et al., 2012; Wu et al., 2017), non-dispersed sediment size was analyzed in this study. The measured PSD of collected sediment samples were divided into 7 particle size classes: 0–0.002 mm, 0.002–0.02 mm, 0.02–0.05 mm, 0.05–0.2 mm, 0.2–0.5 mm, 0.5–1 mm and 1–2 mm.

2.3.3. Flow hydrodynamic parameters

Surface rill flow velocity (V_s ; m s^{-1}) was measured by the stain tracer method, and the average flow velocity (V ; m s^{-1}) in rill cross section was calculated as follows:

$$V = \alpha V_s \quad (3)$$

where α is the flow rate coefficient which takes 0.75 in this experiment (Luk and Merz, 1992; Niu et al., 2020).

The average runoff depth (h ; m) was calculated by:

$$h = Q / (V b t) \quad (4)$$

where V is the average flow velocity (m s^{-1}); t is the duration of collecting a runoff sample (s); Q is the discharge during t (m^3); b is the width of water-crossing section (m).

Reynolds number (Re) and Froude number (Fr), reflecting the rill flow regime, were calculated by:

$$Re = VR/v \quad (5)$$

$$Fr = V / \sqrt{gh} \quad (6)$$

where V is the average flow velocity (m s^{-1}); R is the hydraulic radius of runoff (m); which can be approximated substituted by runoff depth h ; v is the viscosity coefficient of water flow motion, ($\text{m}^2 \text{s}^{-1}$); h is runoff depth (m); g is the acceleration of gravity.

The resistance to rill flow was estimated by Darcy–Weisbach resistance coefficient (f) and Manning roughness coefficient (n), which were calculated by:

$$f = 8ghJ/V^2 \quad (7)$$

$$n = \frac{R^{2/3} J^{1/2}}{V} \quad (8)$$

where g is the acceleration of gravity, being $9.8 (\text{m s}^{-2})$; h is runoff depth (m); J is the surface slope (m m^{-1}); V is average flow velocity (m s^{-1}); R is hydraulic radius (m).

Flow shear stress (τ , N m^{-2}), stream power (ω , $\text{N m}^{-1} \text{s}^{-1}$) and unit stream power (φ , m s^{-1}) were used to describe the hydraulic condition of rill flows, which were calculated by the expressions:

$$\tau = \gamma R J \quad (9)$$

$$\omega = V \tau \quad (10)$$

$$\varphi = V J \quad (11)$$

where γ is the bulk density of water, generally takes $9.8 \times 10^3 (\text{N m}^{-3})$; R is hydraulic radius (m), which is approximately substituted by the runoff depth h ; J is the surface slope (m m^{-1}); V is the average flow velocity (m s^{-1}); τ is the flow shear stress (N m^{-2}).

Relationships between hydrodynamic parameters and rill erosion rate were analyzed and simulated using a method of separate regression, and their determination coefficients were used to assess the goodness of fit.

2.3.4. Morphological characteristics of rills

In this study, the dimensionless parameter width-to-depth ratio C was used to characterize the cross-sectional morphological characteristics of the rill (Ou et al., 2021). The width-to-depth ratio is the ratio of the width of the rill to its depth. The larger the C value is, the closer the rill cross-sectional shape is to the “wide-shallow” shape; while the smaller the C value is, the closer the rill cross-sectional shape is to the “narrow-deep” shape (Bruno et al., 2008).

3. Results

3.1. Runoff and soil loss

3.1.1. Runoff and sediment processes

From the perspective of runoff generating processes, the runoff rate of *UDS* increased rapidly to a certain value at the initial stage (about 0–7 min), then remained stable or had small fluctuations (Fig. 3). While in most cases, the runoff rate of *UDQ* increased more slowly with a smaller increasing range and reached stability later than *UDS*. The runoff rate of *UDS* in the 30th minute increased by 18.1%, 95.7%, 87.0%, 89.4%, 91.4%, respectively; while the runoff rate of *UDQ* in the 30th minute increased by 81%, 80.3%, 86.9%, 44.5%, 42.4%, respectively.

From the perspective of sediment yield processes, sediment yield rates increased and decreased rapidly in early stages, and then decreased slowly to stabilize (Fig. 3). The sediment yield rate peak value of *UDS* appeared at the 6th to 7th minute, except that under the inflow rate of $8.5 \text{ L min}^{-1} \text{m}^{-1}$, which erosion amounts were small and changes were not obvious. Under the inflow rate of $14.5 \text{ L min}^{-1} \text{m}^{-1}$ and $8.5 \text{ L min}^{-1} \text{m}^{-1}$, the sediment yield rate of *UDQ* peaked at the middle and late stage, respectively; under other inflow rates, the peak value appeared at the 3rd minute. It can be seen that the sediment yield rates of *UDS* and *UDQ* mostly peaked at initial stages, and the peak value of *UDQ* appeared earlier than that of *UDS* in most cases. In addition, the peak value of *UDS* was much higher than that of *UDQ* mostly, and there were more fluctuations during the sediment yield processes of *UDS* which indicated its less stable rill development processes.

3.1.2. Variations of runoff and sediment yield rates

Under the inflow rate of 8.5 , 10 and $14.5 \text{ L min}^{-1} \text{m}^{-1}$, the average runoff rate of *UDS* was 1.06 – 1.14 times that of *UDQ* (Fig. 4-a). While the runoff rates of *UDS* and *UDQ* were close under the inflow rate of 11.5 and $13 \text{ L min}^{-1} \text{m}^{-1}$. And the runoff rate variation magnitude of *UDS* was generally smaller than that of *UDQ*. It can be seen that the runoff generation capacity of *UDS* slope was slightly stronger than of *UDQ* slope. Except for the treatment under the inflow rate of $8.5 \text{ L min}^{-1} \text{m}^{-1}$, the sediment yield rate of *UDS* was significantly larger than of *UDQ* ($p < 0.05$) and the average sediment yield rate of *UDS* was 2.26 – 4.71 times that of *UDQ* (Fig. 4-b). Also, the sediment yield rate variation magnitude of *UDS* was relatively larger than that of *UDQ*. It can be seen that the soil loss and rill erosion degree on *UDS* slope was more severe than on *UDQ* slope.

The runoff rates, sediment yield rates and inflow rates fitted well in linear relationships, as expressed using the following equations:

$$RR_S = 0.65IR^{**} - 0.94(R^2 = 0.991) \quad (12)$$

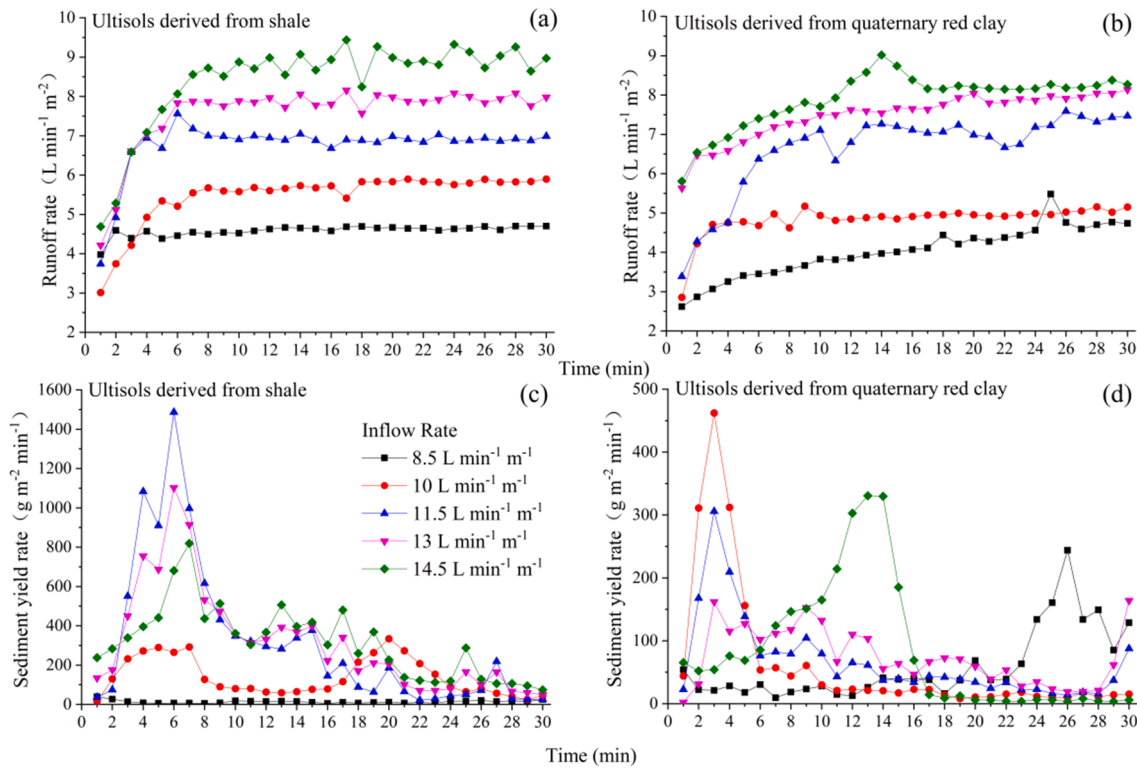


Fig. 3. Temporal variations in the runoff rates and sediment yield rates of two red soils under different inflow rates.

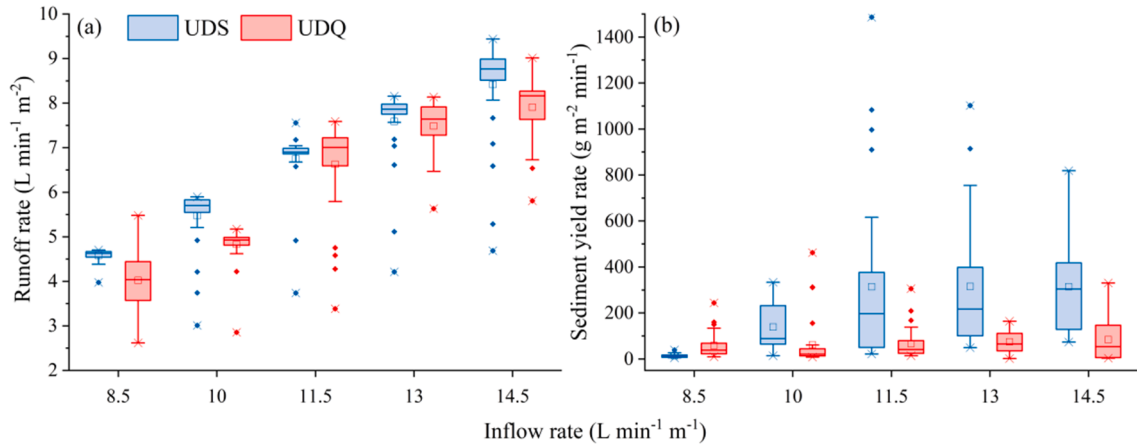


Fig. 4. Box-plot of runoff rates and sediment yield rates of two red soils under different inflow rates. The boxes indicate the 25th and 75th percentiles; the line in the box indicates the median (50th percentile); “ \times ” indicates max–min values; “ \square ” indicates the average value.

$$RR_Q = 0.70IR^{**} - 1.82(R^2 = 0.942) \quad (13)$$

$$SYR_S = 51.85IR^* - 377.07(R^2 = 0.728) \quad (14)$$

$$SYR_Q = 4.21IR^{**} + 20.68(R^2 = 0.941) \quad (15)$$

where RR_S and RR_Q are the runoff rates of *UDS* and *UDQ*, respectively ($L\ min^{-1}\ m^{-2}$); SYR_S and SYR_Q are the sediment yield rates of *UDS* and *UDQ*, respectively ($g\ m^{-2}\ min^{-1}$); IR is inflow rate ($L\ min^{-1}\ m^{-1}$); * represents significance at $p < 0.05$ level; ** represents significance at $p < 0.01$ level.

The runoff rates of *UDS* and *UDQ* were both positively correlated with the inflow rate ($p < 0.01$), which indicated that large upslope inflow rate promoted runoff generation. Also, the sediment yield rates of *UDS* and *UDQ* were positively correlated with the inflow rate ($p < 0.05$

and 0.01 , respectively), which indicated that the increase of inflow rate aggravated soil erosion degree on red soil slopes. The sediment yield rate of *UDQ* increased steadily and slowly with inflow rate; while the sediment yield rate of *UDS* increased faster as the inflow rate increased from $8.5\ L\ min^{-1}\ m^{-1}$ to $11.5\ L\ min^{-1}\ m^{-1}$, and then did not change obviously. It can be seen that the promotion effect of inflow rate on sediment yield was rather strong for *UDS* until it increased to some high value, and *UDQ* was less sensitive to inflow rate changing.

3.2. Particle size distribution of eroded sediments

3.2.1. Temporal variations of non-dispersed sediment size

Fig. 5 showed the temporal variation process in sediment particle size distribution of *UDS* and *UDQ* under different inflow rates. During all

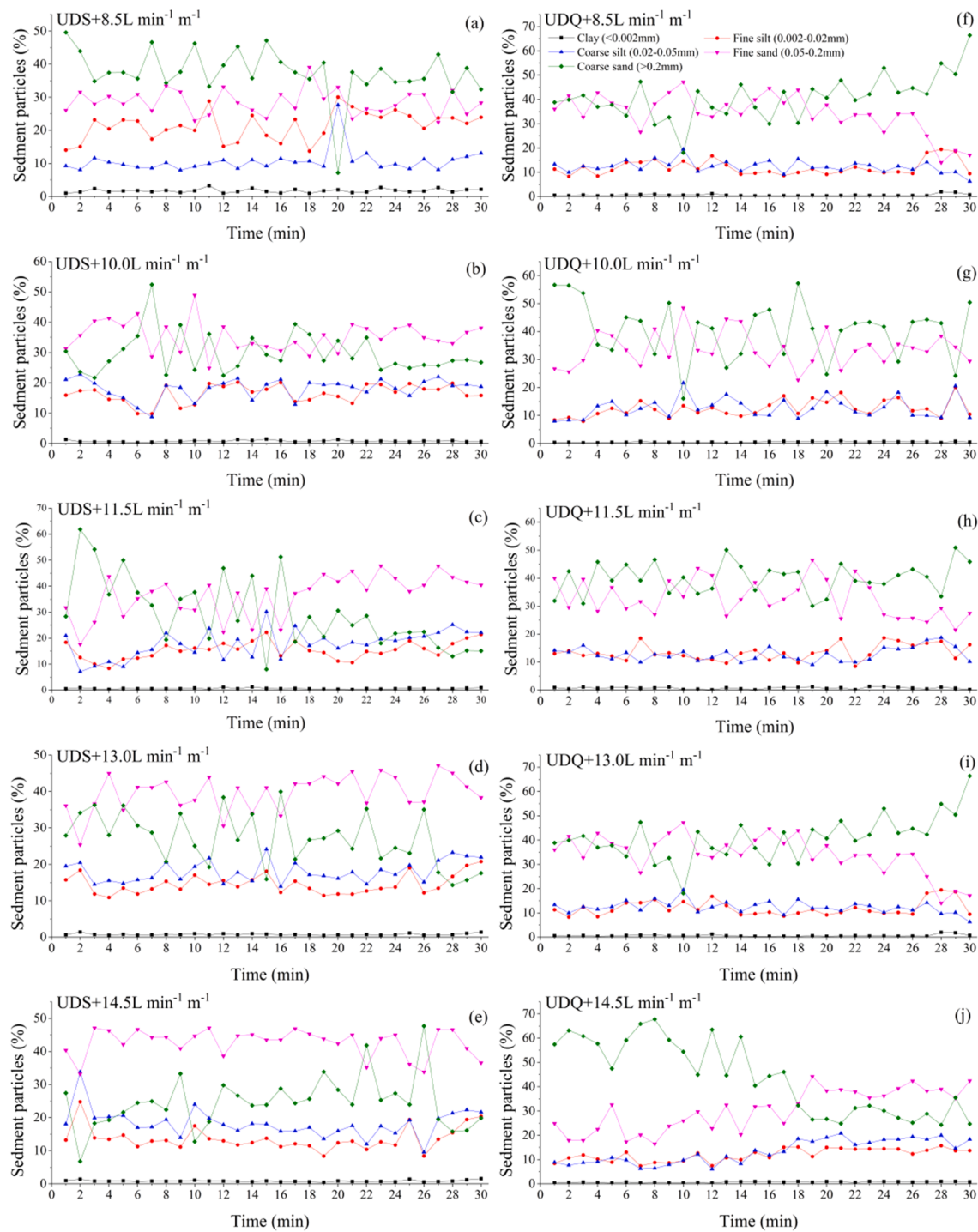


Fig. 5. Changes in the percentage of sediment particles with time.

the processes of experiments, the percentage of clay (<0.002 mm) stayed almost unchanged (basically between 0 and 4%) with the prolongation of time, indicating that the clay particles dispersed by runoff did not increase during the process of rill erosion and the clay dispersion seldom occurred in the process rill flow movement, which was consistent with the findings of Shi et al. (2012) and Tang et al. (2017). With the increase of scouring time, the percentages of fine silt and coarse silt were basically stable, and the two were very close; while the percentages of fine and coarse sand obviously fluctuated, and the sum of them remained relatively steady.

In order to investigate the dynamic changes of sediment size

distribution in different rill erosion stages, the eroded sediments in three different periods were selected (the 2–5 min: rill initiation stage; the 13–16 min: rill development stage; the 24–27 min: rill stable stage), shown in Fig. 6.

The sediment PSD varied in different stages of rill erosion, and presented as unimodal distribution with the peak at 0.05–0.2 mm (fine sand) or bimodal distribution with peaks at 0.05–0.2 mm and 0.2–0.5 mm. In the three erosion stages under all five inflow rates, the fraction of fine sand in sediment varied over the ranges of 27.27–44.20% and 22.71–50.55% for UDS and UDQ, respectively. Based on the results of paired sample *T* test, the >0.02 mm size fraction content (74.34–90.38%)

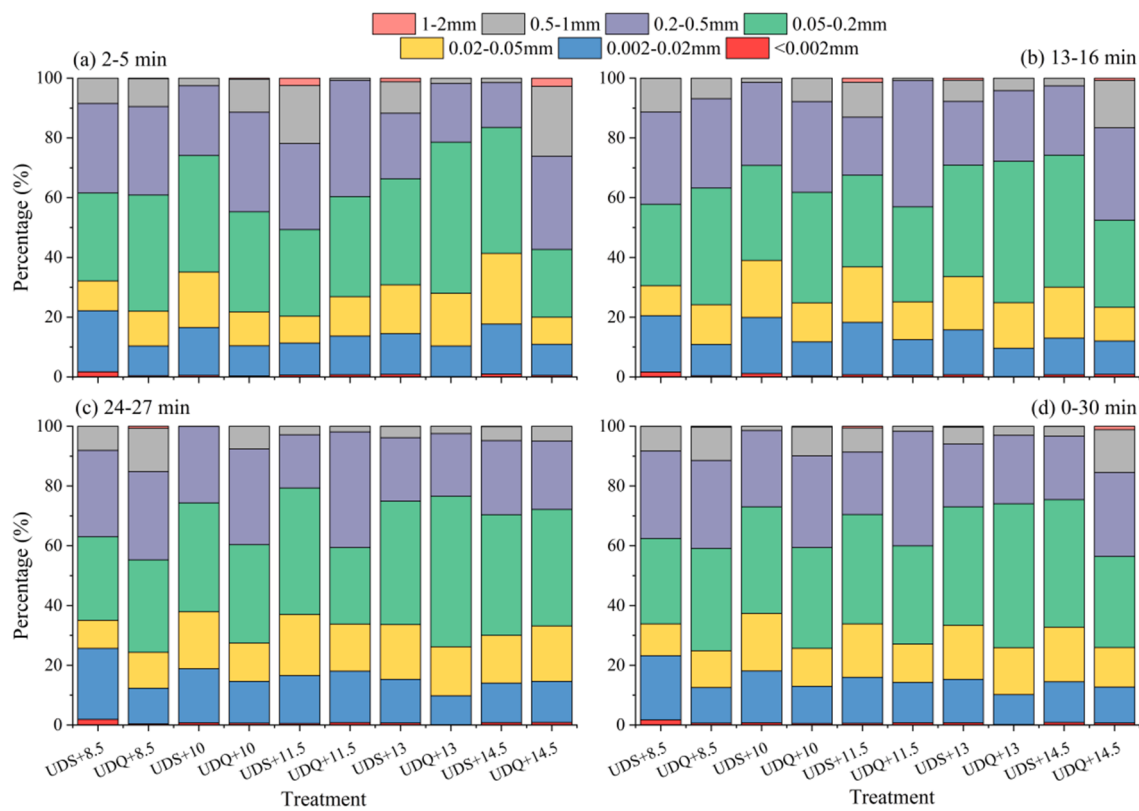


Fig. 6. Sediment size distribution at 2–5 min (a), 13–16 min (b), 24–27 min (c) and 0–30 min (d). UDS + n, UDQ + n referred to the sediment particle size distribution of UDS and UDQ under the inflow rate of n $\text{L min}^{-1} \text{m}^{-1}$, respectively.

was significantly higher than the $< 0.02 \text{ mm}$ fraction content (9.62–25.65 %) in the three erosion stages ($P < 0.05$). In most cases, both the fine ($< 0.02 \text{ mm}$) and coarse ($> 0.2 \text{ mm}$) particles took larger proportions in sediments during the rill development and stable stages than during the rill initiation stage.

3.2.2. Particle size distributions of the total eroded sediments

According to Fig. 6d, the sediment was principally composed of sand (0.05–2 mm) which took the proportions of 62.65%–67.22% and 72.91%–75.12% in the total eroded sediments of UDS and UDQ, respectively, much higher than the sand contents of 19.70% and 4.41% in the original soil samples. Subsequently, the silt fractions accounted for 31.94%–36.58% and 24.23%–26.36% in the total outlet sediments of UDS and UDQ, respectively, which were lower than their proportions of 56.77% and 60.52% in the original soil samples. Despite clay contents of 23.53% and 35.07% for the original soil samples of UDS and UDQ, 0.60%–1.74% and 0.15%–0.72% of the total sediments were $< 0.002 \text{ mm}$. Both of the two red soils were shown as the enrichment of sand particles, indicating the preferentially transportation of sand by rill flow.

According to the *independent sample T-test* results, there were differences in the eroded sediment particle compositions of UDS and UDQ. Under the same inflow rate, the silt content in UDS was significantly larger than that in UDQ, while the sand content in UDS was significantly smaller than that in UDQ ($p < 0.05$). Under the inflow rate of $11.5 \text{ L min}^{-1} \text{m}^{-1}$, the clay contents in the eroded sediments of UDS and UDQ were not significantly different, while under the remaining four inflow rates, the clay content in the eroded sediments of UDS was significantly higher than that of UDQ ($p < 0.05$). In more specific sediment size distribution, the proportions of coarse particles with size $> 0.2 \text{ mm}$ in UDQ were 3.30%, 13.63%, 10.49% and 19.04% larger than in UDS under the inflow rate of 8.5, 10, 11.5 and $14.5 \text{ L min}^{-1} \text{m}^{-1}$, respectively. While the proportions of fine particles with size $< 0.02 \text{ mm}$ in UDS were 10.68%, 5.12%, 1.72%, 5.10% and 1.81% larger than in UDQ

under the inflow rate of 8.5, 10, 11.5, 13 and $14.5 \text{ L min}^{-1} \text{m}^{-1}$, respectively.

3.3. Flow hydrodynamics

3.3.1. Spatiotemporal variations of flow velocities

From Fig. 7, flow velocity distributions on UDS and UDQ slopes were both shown as the middle and lower slopes faster and the upper slope slower, but the flow velocity of UDQ was slower than that of UDS under the same inflow rate. In addition, with the increase of inflow rate, the flow velocity of UDS at the lower slope exceeded that at the middle slope gradually, while the flow velocity of UDQ at the middle slope exceeded that at the lower slope gradually. This was related to the differences in surface roughness and erosion resistance caused by soil texture, and the rill morphology during its development process.

Fig. 8 shows that on UDS and UDQ slopes, the flow velocities increased and decreased rapidly in the early stages, and tended towards a fluctuating-steady state in the middle and late stages. The difference is that the flow velocities on UDS slopes rose again in the middle stages and the fluctuation range was larger during the whole process. In addition, the flow velocities on UDQ slopes reached peak value (the 1st to 3rd minute) earlier than on UDS slopes (the 7th to 9th minute), which was because on UDQ slopes, the soil moisture reached saturation through infiltration faster or rills occurred earlier. In the process of runoff scouring, the changing trends of sediment yield rate and velocity with time were basically consistent, and the change of flow velocity was synchronous or slightly lagging behind the change of sediment yield rate (Figs. 3 and 8).

3.3.2. Variations of other hydrodynamic parameters

For UDS and UDQ, both mean rill flow velocity (V) and flow depth (h) increased with the inflow rate, and the V and h values of UDS were basically higher than that of UDQ (Table 2).

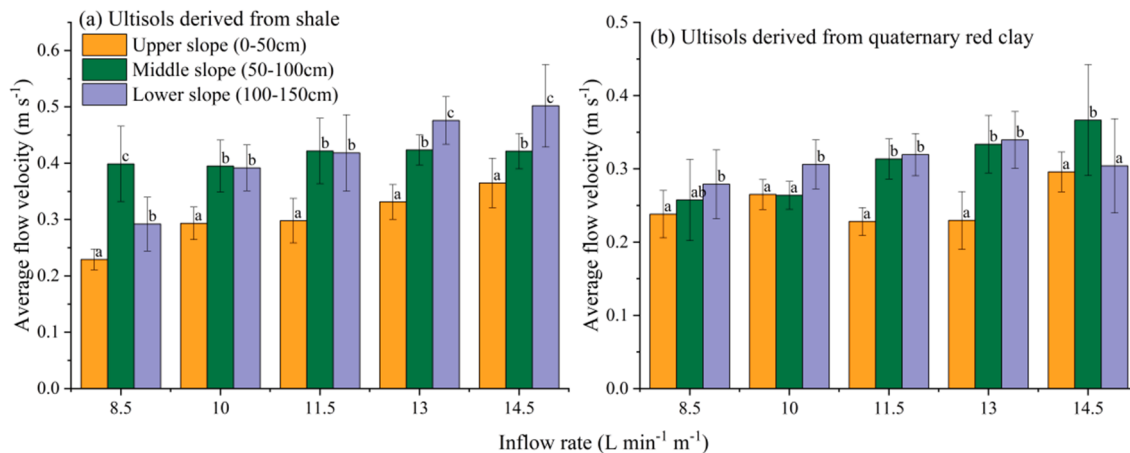


Fig. 7. Average flow velocity at different slope sections during the whole experiment process under different inflow rates. Values for different slope sections in the same treatment followed by different letters (a, b and c) are significantly different at $p < 0.05$ according to the LSD test.

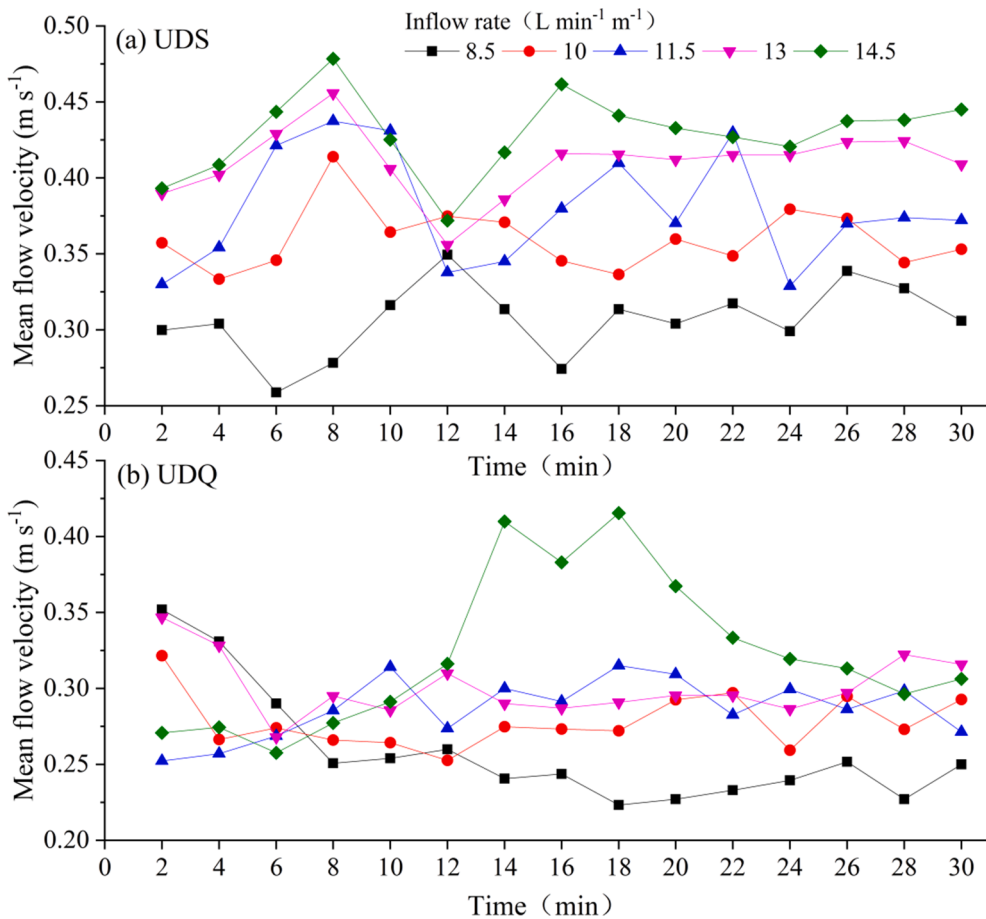


Fig. 8. Temporal variations in the mean flow velocities of two red soils under different inflow rates. Mean flow velocity: the average flow velocity on the whole slope; UDS: Ultisols derived from shale; UDQ: Ultisols derived from quaternary red clay.

The average rill flow Re of UDS and UDQ varied from 2450.40 to 4321.81 and 1395.57–2613.10, respectively, and showed an increase trend with inflow rate. All the Re of UDS were >2000 , indicating a turbulent flow; while the rill flow on UDQ slopes gradually switched from transitional flow to turbulent flow as the inflow rate increased. On UDS slope under the inflow rate of $8.5 \text{ L min}^{-1} \text{ m}^{-1}$, where no rills obviously generated, the average overland flow Re was 257.44, indicating a laminar flow. The average rill flow Fr of UDS and UDQ varied from 1.33

to 1.59 and 1.05–1.17, respectively, and all of them were >1 , which indicated a supercritical flow; however, they were all significantly lower than the average overland flow Fr of 3.38 on UDS slope under the inflow rate of $8.5 \text{ L min}^{-1} \text{ m}^{-1}$. In addition, the Fr and Re values of UDS were basically higher than that of UDQ under the same inflow rate.

For rill flow on UDS and UDQ slopes, the f varied from 0.73 to 1.00 and 1.10–1.45, respectively, and the n varied from 0.04 to 0.05 and 0.05–0.06, respectively, and all of them showed an increase trend with

Table 2

Slope flow hydraulic parameters for different inflow rates and soil types.

Soil type	Inflow rate ($\text{L min}^{-1} \text{m}^{-1}$)	V (m s^{-1})	h (mm)	Re	Fr	f	n	τ (N m^{-2})	ω ($\text{N m}^{-1} \text{s}^{-1}$)	φ (m s^{-1})
UDS	8.5	0.31 ± 0.02	$0.95 \pm$	$257.44 \pm 6.51\text{a}$	$3.38 \pm$	$0.16 \pm$	$0.01 \pm$	$1.31 \pm$	$0.37 \pm$	0.04 ± 0.00
		cd	0.08a		0.40d	0.07a	0.00a	0.12a	0.01a	cd
	10	$0.36 \pm$	$7.40 \pm$	$2450.40 \pm$	$1.39 \pm$	$0.73 \pm$	$0.04 \pm$	$10.19 \pm$	$3.56 \pm$	$0.05 \pm$
		0.02e	0.98c	298.64e	0.14b	0.16b	0.01b	1.35c	0.43e	0.00e
	11.5	$0.38 \pm$	$9.25 \pm$	$3162.04 \pm$	$1.33 \pm$	$0.90 \pm$	$0.05 \pm$	$12.74 \pm$	$4.59 \pm$	$0.05 \pm$
		0.04e	1.04e	317.32f	0.18b	0.21bc	0.01c	1.43e	0.46f	0.01e
	13	$0.41 \pm$	$11.48 \pm$	$4049.59 \pm$	$1.45 \pm$	$1.00 \pm$	0.05 ± 0.01	$15.82 \pm$	$5.88 \pm$	$0.06 \pm$
		0.02f	1.58f	459.34 g	0.13bc	0.24c	cd	2.18f	0.67 g	0.00f
	14.5	$0.43 \pm$	$11.73 \pm$	$4321.81 \pm$	$1.59 \pm$	$0.92 \pm$	$0.05 \pm$	$16.15 \pm$	$6.28 \pm$	$0.06 \pm$
		0.03f	2.00f	572.85 h	0.14c	0.29bc	0.01c	2.76f	0.83 h	0.00f
UDQ	8.5	$0.26 \pm$	$5.95 \pm$	$1395.57 \pm$	$1.13 \pm$	$1.15 \pm$	0.05 ± 0.01	$8.20 \pm$	$2.03 \pm$	$0.04 \pm$
		0.04a	1.46b	220.96b	0.37a	0.46c	cd	2.01b	0.32b	0.01a
	10	$0.28 \pm$	$7.42 \pm$	$1947.03 \pm$	$1.05 \pm$	$1.10 \pm$	$0.05 \pm$	$10.22 \pm$	$2.83 \pm$	$0.04 \pm$
		0.02b	0.81c	151.32c	0.15a	0.22c	0.01d	1.12c	0.22c	0.00b
	11.5	$0.29 \pm$	8.15 ± 1.02	$2166.54 \pm$	$1.05 \pm$	1.26 ± 0.16	$0.06 \pm$	$11.22 \pm$	$3.15 \pm$	$0.04 \pm$
		0.02bc	cd	340.50d	0.08a	cd	0.00de	1.40d	0.49d	0.00bc
	13	$0.30 \pm$	$8.43 \pm$	$2193.74 \pm$	$1.17 \pm$	$1.45 \pm$	$0.06 \pm$	$11.61 \pm$	$3.19 \pm$	$0.04 \pm$
		0.02c	1.11d	171.91d	0.14a	0.45d	0.01e	1.53de	0.25d	0.00c
	14.5	$0.32 \pm$	$8.88 \pm$	$2613.10 \pm$	$1.14 \pm$	$1.11 \pm$	$0.05 \pm$	$12.23 \pm$	$3.80 \pm$	$0.05 \pm$
		0.05d	0.86de	227.07e	0.25a	0.33c	0.01d	1.18e	0.33e	0.01d

V : average flow velocity; h : average runoff depth; Re : Reynolds number; Fr : Froude number; f : Darcy–Weisbach resistance coefficient; n : Manning roughness coefficient; ω : stream power; τ : flow shear stress; φ : unit stream power. Hydraulic parameter values for different treatments followed by different letters (a, b, c, e, f, g and h) are significantly different at $p < 0.05$ according to the LSD test.

inflow rate (Table 2). And on *UDS* slope under the inflow rate of $8.5 \text{ L min}^{-1} \text{m}^{-1}$, the overland flow f and n were 0.16 and 0.01, respectively, which were significantly lower than the f and n of rill flow. The f and n values of *UDQ* were basically larger than that of *UDS*. Moreover, the minimum f value of *UDQ* was still larger than the maximum value of *UDS*.

In the rills of *UDS* and *UDQ*, the flow shear stress (τ) varied from 10.19 to 16.15 N m^{-2} and 8.20 – 12.23 N m^{-2} respectively, the stream power (ω) varied from 3.56 to $6.28 \text{ N m}^{-1} \text{s}^{-1}$ and 2.03 – $3.80 \text{ N m}^{-1} \text{s}^{-1}$ respectively, the unit stream power (φ) varied from 0.05 to 0.06 m s^{-1} and 0.04 – 0.05 m s^{-1} respectively. All of them showed an increase trend with inflow rate, and are significantly higher than the overland flow τ , ω and φ of 1.31 N m^{-2} , $0.37 \text{ N m}^{-1} \text{s}^{-1}$ and 0.04 m s^{-1} on *UDS* slope under the inflow rate of $8.5 \text{ L min}^{-1} \text{m}^{-1}$. In addition, the τ , ω and φ values of *UDS* were basically higher than that of *UDQ*, and the increasing range of τ and ω with the inflow rate was larger for *UDS*.

Overall, most of the hydraulic parameters increased with the inflow rate. The f and n values were higher for *UDQ*, while other parameters were basically higher for *UDS*, indicating a higher rill flow resistance for *UDQ* but a higher erosive force for *UDS*. Also, it can be seen that the occurrence and development of rills on red soil slopes had significant impact on the hydraulic characteristics of slope flow, which showed as its increase in the turbulence, resistance, erosive force and energy.

3.4. Rill erosion characteristics

3.4.1. Rill morphology

Rill width and depth measurements were conducted at 6 cross sections that were uniformly distributed along each rill channel from top to bottom, which was illustrated in Fig. 9.

The upper rill sections on *UDQ* slope were relatively narrow and shallow mostly, and the rills became wider at middle and lower sections, but the depth of rills did not change much or became shallower at the lower section (Fig. 10b), except for the rill depth under the inflow rate of $14.5 \text{ L min}^{-1} \text{m}^{-1}$ which increased obviously with slope length. While the upper rill sections on *UDS* slope were relatively wide and deep mostly, and at the middle section, the width of rills decreased, the depth decreased slightly and still remained relatively high value, and the rills turned to “wide and shallow type” at the lower section (Fig. 10a). On *UDS* and *UDQ* slopes, the rills gradually became wider and shallower at

the lower section in most cases, which might be explained as follows. At the upper section, due to the smaller amounts of sediments carried by runoff, the power of downward and headward erosion was stronger. As runoff flowing downward slope, the amounts of sediments carried by runoff increased gradually, so the erosive and transport power of runoff became weaker, and sediments gradually deposited at the lower section, which widen the rills gradually and enlarged the erosion surface. This was similar to the development principle of river geomorphology (Ma et al., 2017).

Overall, the rill width of *UDQ* ranged between 1.7 and 6.9 cm with an average of 3.63 cm , and the rill width of *UDS* ranged between 2.3 and 6.1 cm with an average of 3.95 cm , which were relatively close. Meanwhile, the rill depth of *UDQ* ranged between 0.4 and 4.4 cm with an average of 1.76 cm , and the rill depth of *UDS* ranged between 1.2 and 11.7 cm with an average of 5.63 cm , which was much deeper. As a result, the rill width-depth ratio of *UDQ* ranged between 0.58 and 7.67 with an average of 2.92 , and the rill width-depth ratio of *UDS* ranged between 0.34 and 3.58 with an average of 0.94 , which was smaller.

3.4.2. Rill erosion amounts

The rill erosion amounts of *UDS* were 0 , 1.42 , 3.22 , 3.45 and 3.49 kg under the inflow rate of 8.5 , 10 , 11.5 , 13 and $14.5 \text{ L min}^{-1} \text{m}^{-1}$, respectively. The rill erosion amounts of *UDQ* were 0.34 , 0.52 , 0.57 , 0.71 and 0.94 kg under the inflow rate of 8.5 , 10 , 11.5 , 13 and $14.5 \text{ L min}^{-1} \text{m}^{-1}$, respectively. Except for the inflow rate of $8.5 \text{ L min}^{-1} \text{m}^{-1}$, the rill erosion amounts of *UDS* were much larger than that of *UDQ*, indicating the more severe rill erosion degree on *UDS* slopes. Rill erosion amounts accounted for 51.95 – 88.45% of soil loss amounts for all treatments, with the average contribution of 77.36% . Also, the contribution of rill erosion amounts showed an increasing trend with inflow rate. The rill erosion amounts and inflow rates fitted well in linear relationships, as expressed using the following equations:

$$REA_S = 0.60IR^* - 4.59(R^2 = 0.788) \quad (16)$$

$$REA_Q = 0.09IR^{**} - 0.44(R^2 = 0.949) \quad (17)$$

where REA_S is the rill erosion amount of *UDS* (kg); REA_Q is the rill erosion amount of *UDQ* (kg); IR is inflow rate ($\text{L min}^{-1} \text{m}^{-1}$); * represents significance at $p < 0.05$ level; ** represents significance at $p < 0.01$

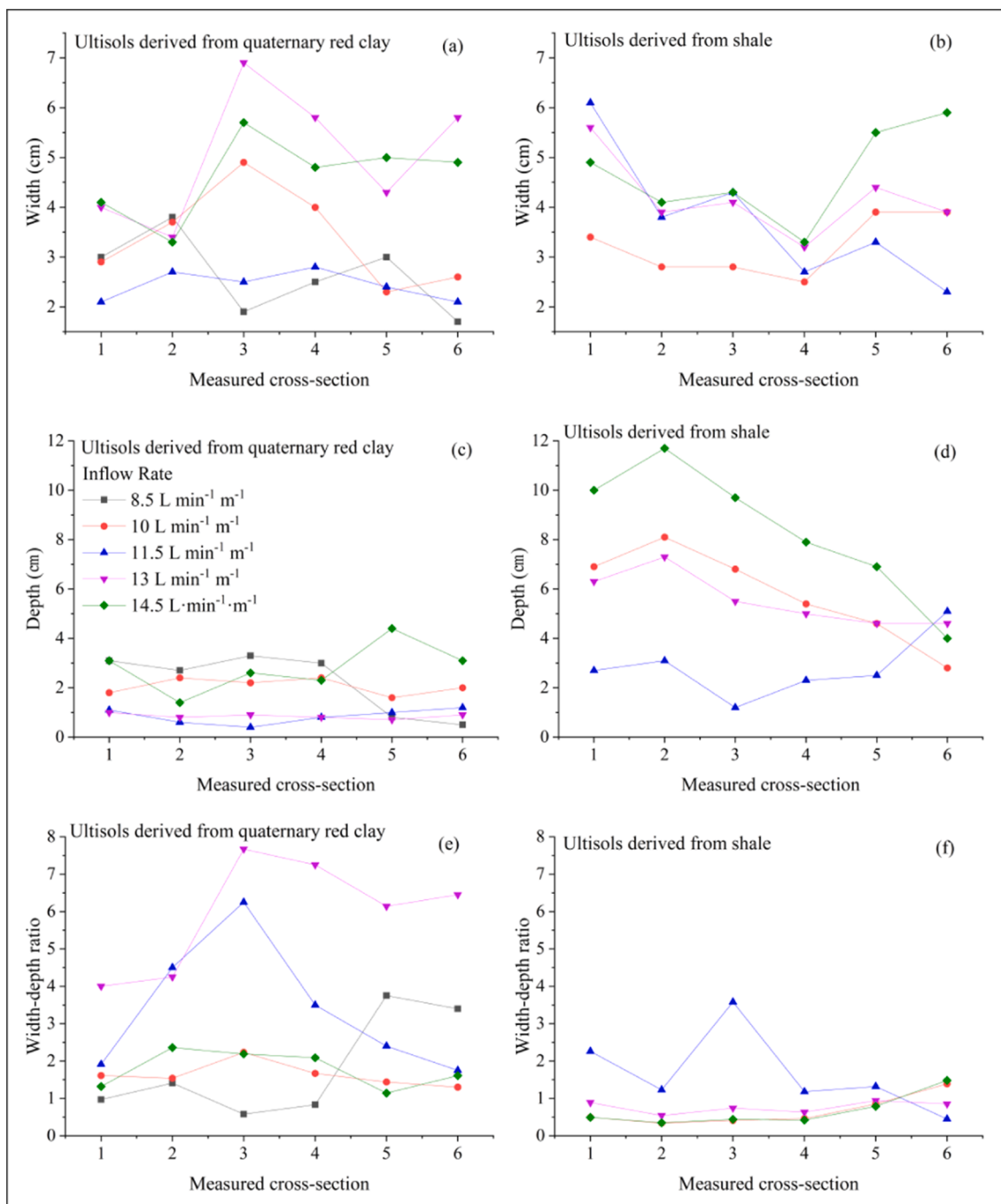


Fig. 9. Rill width, depth and width-depth ratio of two red soils under different inflow rates. Measured cross-sections were uniformly distributed along each rill channel from top to bottom and there was no obvious rill generated on the UDS slope under the inflow rate of $8.5 \text{ L min}^{-1} \text{m}^{-1}$.

level.

The rill erosion amounts of *UDS* and *UDQ* were both positively correlated with the inflow rate ($p < 0.05$ for *UDS*; $p < 0.01$ for *UDQ*), which indicated the increase of runoff erosivity with inflow rate caused more severe hillslope rill erosion. Additionally, the increments of rill erosion amounts with inflow rate were larger for *UDS* than *UDQ*.

4. Discussion

4.1. Factors influencing rill morphology

The reasons for the differences in the rill morphology of the two red soils might be explained as follows. *UDS* with higher sand content was

more vulnerable to water erosion and the erosion process was more unstable, leading to its larger erosion depth and variation range. While many water-stable micro-aggregates in *UDQ* with clayey texture strengthened the soil anti-erodibility and enlarged the surface resistance (Ma et al., 2014; Wei et al., 2015), leading to its weaker rill erosion degree than that of *UDS*. As a result, the rill depth of *UDQ* was basically smaller with the minimum of 0.4 cm, making its larger rill width-depth ratio with the maximum of 7.67. However, Zhao and Gao (2016) indicated that the rill width-depth ratio of soils with finer texture appeared to be smaller through comparing the field investigation results of different researchers. Also, Ou et al. (2021) found that soils with higher clay content appeared to form narrower and deeper rills under the same manner of erosive force. This discrepancy may be related to the

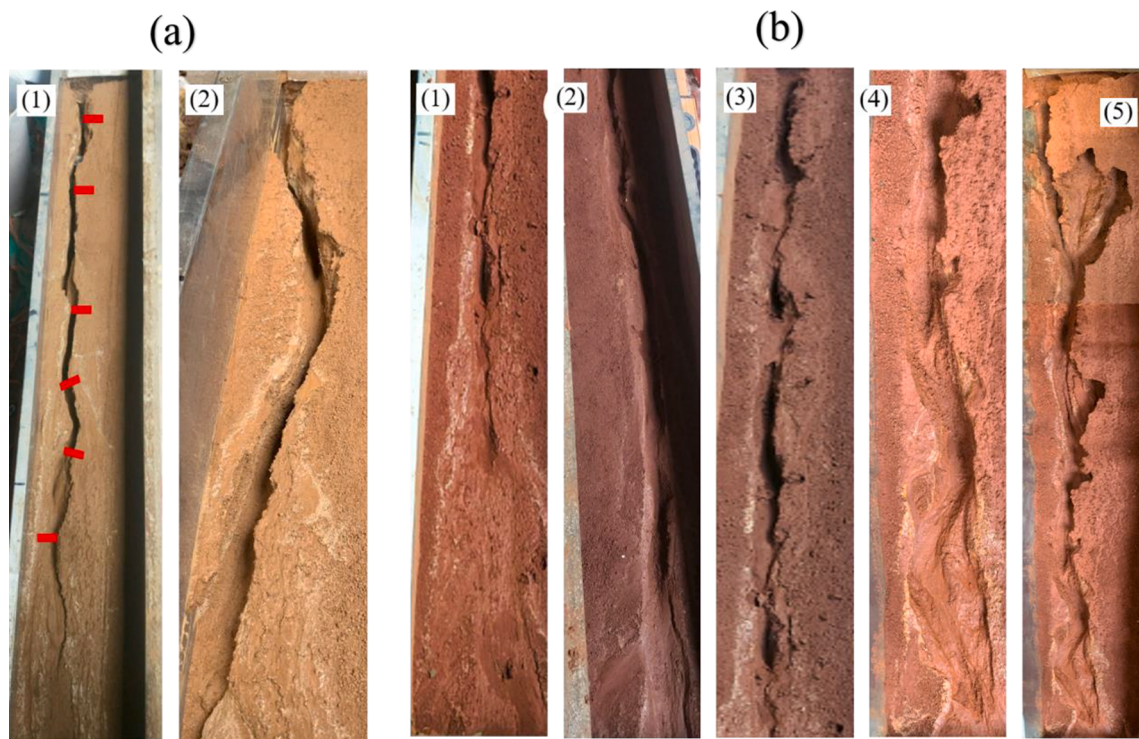


Fig. 10. The rills developed on *UDS* slope (a) and *UDQ* slope (b) under different inflow rates. a: $10.0 \text{ L min}^{-1} \text{ m}^{-1}$ (1), $13.0 \text{ L min}^{-1} \text{ m}^{-1}$ (2); b: $8.5 \text{ L min}^{-1} \text{ m}^{-1}$ (1), $10.0 \text{ L min}^{-1} \text{ m}^{-1}$ (2), $11.5 \text{ L min}^{-1} \text{ m}^{-1}$ (3), $13.0 \text{ L min}^{-1} \text{ m}^{-1}$ (4), and $14.5 \text{ L min}^{-1} \text{ m}^{-1}$ (5).

differences in laboratory and field experimental conditions and the specific variables selected in the experiment.

4.2. Relationships between flow velocity and rill morphology

In rill erosion processes, flow velocity was affected by gravity action and rill morphology. The increase of rill width made rill flow become shallower and more susceptible to the rill bottom shape, which caused the resistance of flow larger and flow velocity slower (Giménez et al., 2001). With the concentration of surface runoff in rills, the deepening of rills caused by downcutting erosion led to the increase of rill flow depth and velocity. For *UDS* and *UDQ*, the flow velocity along rill channel was faster at the middle and lower section, and slower at the upper section. The rill morphology in this experiment mainly showed as the upper section surface widening, middle section deeper and lower section shallower (Fig. 10).

On *UDS* slope, the flow velocity at the middle section was much larger than that at the upper and lower section under the inflow rate of $8.5 \text{ L min}^{-1} \text{ m}^{-1}$, and with the increase of inflow rate, the flow velocity at the lower section gradually exceeded that at the middle section. This resulted from no rills generated on *UDS* slope under the inflow rate of $8.5 \text{ L min}^{-1} \text{ m}^{-1}$, and partial runoff infiltrated and transformed to interflow at the lower section, which decreased the water flow thickness and increased resistance. Under other inflow rates, although the lower sections of rills were wider and shallower compared with the upper and middle sections, the rills at this section were still relatively deep. Thus, the influence of rill morphology on flow velocity was smaller than that of gravity action and the flow velocity generally increased down slope.

While for *UDQ*, the rills were basically wider and shallower than those of *UDS* and they mainly developed at the upper and middle sections (Fig. 10b). This was because that stable rills were firstly developed at the upper and middle slope in the scouring process, and the down-cutting erosion became weaker gradually and partial eroded sediments deposited when the rills extended downslope. As a result, with the extension downslope, rills gradually became shallower, and the

sediment concentration and resistance in rill flow increased. Therefore, on *UDQ* slope, the flow velocity at the lower section increased slowly with inflow rate. While at the middle section where rill developed obviously, the runoff was deeper and more concentrated, and the flow velocity increased faster and gradually exceeded that at the lower section with the increase of inflow rate, which was contrary with *UDS*.

4.3. Sediment sorting and transport mechanisms

4.3.1. Sediment sorting mechanisms

Sand particles were enriched in the total eroded sediments of the two red soils, which was consistent with Wan and El-Swaify (1997), who found sand particles ($>0.05 \text{ mm}$) enriched in the eroded sediments of oxisol when runoff velocity was fast and rills were generated. According to Imhoff et al. (2002), clay and silt fractions ($<0.05 \text{ mm}$) acted as cementing agent in water stable aggregate formation. Wei et al. (2016) suggested that fine particles ($<0.05 \text{ mm}$) jointly contributed to aggregate water stability against slaking while coarse particles ($>0.05 \text{ mm}$) played the inverse role. And Lu et al. (2014) found the pore structure of Ultisols greatly influenced by clay. It can be seen that fine particles ($<0.05 \text{ mm}$) played an important role in the original soil structure and aggregate stability. In this study, fine particles ($<0.05 \text{ mm}$) accounted for 80.30% and 95.59% in the original soil samples of *UDS* and *UDQ*, respectively, which made the aggregates with rather high water stability more difficult to be broken down by runoff scouring. In addition, the concentrated flow in rills with high flow depth, velocity and erosive power, was able to detach and transport relatively large particles. Thus, coarse particles ($>0.05 \text{ mm}$) were enriched in the eroded sediments.

The clay content in the total eroded sediments was much lower than in the original soil samples. That's because clay-sized particles were commonly associated with aggregation by rearrangement and flocculation (Bronick and Lal, 2005), and clays became available for transport when flow energy was high enough to destroy soil aggregates (Durnford and King, 1993). In terms of the hierarchical nature of soil structure, as well as the cohesion and stability in soil aggregates, large aggregates are

stepwise destroyed into smaller aggregates rather than clay or silt particles under runoff scouring (Wei et al., 2016). Thus, the clay content was rather low for many clay particles existing in aggregates during the process of rill erosion.

The differences mainly showed as higher silt content and lower sand content in the eroded sediments of *UDS* than *UDQ*, which was similar to the findings of Wu et al. (2014). Yang et al. (2016) found coarse particles enriched in the eroded sediments of *UDQ* and most of them were stable aggregates. Meyer et al. (1992) reported that eroded sediments of clay loam and silty clay loam mainly existed in the form of granular, and the particle size was larger; while Shi et al. (2017) found that the eroded sediments of silt loam soil with medium texture most existed in the form of primary particle and the particle size was smaller. And Wu et al. (2018) suggested that clay content exerted a positive role in sediment size, due to the large cohesive forces between particles against slope flow destruction. Therefore, the reason for the differences in the PSD of the two red soils might be attributed to the difference in soil texture and the different aggregate stability caused by it. The higher clay content in *UDQ* enhanced the anti-dispersion ability of wet soil layer and aggregate stability, leading to its relatively weaker dispersion of runoff to aggregates, and the higher content of coarse particles (>0.05 mm) in eroded sediments.

As for different rill erosion stages, both the fractions of fine (<0.02 mm) and coarse (>0.2 mm) particles were larger in the rill development and stable stages than the rill initiation stage in most cases, which was consistent with the results obtained by Shi et al. (2012) and Hao et al. (2019). According to Young (1980), particles and aggregates with size between 0.02 and 0.20 mm were more erodible, because the movement of particles with size >0.20 mm was limited by their enough mass, and the detachment of particles <0.02 mm was impeded by cohesive forces. This indicated that as rill developing, the concentrated flows in rills with higher energy were able to break down more soil aggregates and detach, transport more particles with size <0.02 mm and >0.2 mm. Therefore, soil texture and rill flow energy played a major role in particle selectivity, in the present study.

4.3.2. Sediment transport mechanisms

Size class with lowest sediment concentration can be used to estimate an approximate cutoff between the two transport mechanisms of suspension–saltation and bed load (rolling) (Asadi et al., 2011; Shi et al., 2012). In this study, the transition from saltating to contact (rolling) load mainly lied in the size range of 0.2–0.5 for *UDS*; while for *UDQ*, the transition mostly lied in the size range of 0.5–1 mm (Fig. 6). Asadi et al. (2011) suggested the boundaries for contact (rolling) load exist for size classes between 0.18 and 0.38 mm in fluvial sand and between 0.5 and 1.0 mm in forest soil. Shi et al. (2012) indicated that the boundaries for rolling load approximated the sediment size of 0.054–0.152 mm for a clay loam soil under rainfall-driven erosion on steep slopes. The upper size limit of particles transported by suspension–saltation depended on both soil texture and flow hydrodynamic characteristics. The relative importance of each mechanism in sediment loss during three rill erosion

stages is calculated and presented in Table 3.

Suspension–saltation mechanism had an important role in particle transport, which took the proportions of 66.33–91.94% and 72.18–93.14% for *UDS* and *UDQ*, respectively (Table 3). However, the importance of suspension–saltation reduced as rill developed on hill-slope, and bed load transport by rolling becomes more active. And the relative effect of sediment transport by contact (rolling) load was higher for *UDS* than *UDQ* under most cases. Sediment transport by contact (rolling) load generally showed an increase trend with inflow rate, which could be attributed to the higher flow energy under large upslope inflow conditions. For *UDS*, 8.06–11.33% of soil particles were transported by contact (rolling) load under the inflow rate of $8.5 \text{ L min}^{-1} \text{ m}^{-1}$ where no obvious rill generated, much lower than that under the remaining four inflow rates. This indicated that the concentration of size fractions associated with rolling transport was higher in rill flows than overland flows.

4.4. Hydrodynamic mechanisms of rill erosion

To analyze the correlations between flow hydrodynamics and rill erosion, five parameters that have good fitting relationships with the rill erosion rate (*RER*) are presented in Fig. 11. For *UDS*, the determination coefficients of fitting functions decreased in the order of $\omega = Re > \tau > V > \varphi$. While for *UDQ*, the determination coefficients decreased in the order of $\varphi > V > Re = \omega > \tau$. For *UDS*, ω and Re are the best hydraulic parameters to describe the rill erosion processes, and for *UDQ*, the optimal hydraulic parameter is φ .

Simple linear regression analysis between *RER* and τ indicated the rill erodibility parameters of $3.5 \times 10^{-4} \text{ s m}^{-1}$ and $1.9 \times 10^{-4} \text{ s m}^{-1}$ for *UDS* and *UDQ*, respectively. Both of them were lower than the rill erodibility parameter of $7.95 \times 10^{-3} \text{ s m}^{-1}$ for a gravelly sandy loam (Nearing et al., 1999), $8.18 \times 10^{-4} \text{ s m}^{-1}$ for a loess (Zhang and Zhang, 2000), and $2.7 \times 10^{-3} \text{ s m}^{-1}$ for a silt loam (Zhang et al., 2015). In addition, the rill erodibility parameter of *UDS* was 1.84 times that of *UDQ*, showing *UDS*'s higher susceptibility to rill erosion.

When no rill erosion occurred, i.e., *RER* = 0, then the critical hydrodynamic force was determined. For *UDS*, the critical τ , ω and φ were 1.31 N m^{-2} , $0.28 \text{ N m}^{-1} \text{ s}^{-1}$ and 0.04 m s^{-1} , respectively, which were slightly higher than the results of 0.986 N m^{-2} , $0.207 \text{ N m}^{-1} \text{ s}^{-1}$ and 0.002 m s^{-1} by Shen et al. (2016). For *UDQ*, the critical τ , ω and φ were 6 N m^{-2} , $1.12 \text{ N m}^{-1} \text{ s}^{-1}$ and 0.03 m s^{-1} , respectively, and the critical τ and ω were much higher than that of *UDS*, indicating that the rill erosion on *UDQ* slope occurred under runoff with higher erosive power.

5. Conclusions

In this study, erosion and rill development processes of two typical red soils (*UDS*, *UDQ*) in subtropical China were systematically investigated with indoor runoff scouring experiments. The results showed that for the two red soils, runoff rate, sediment yield rate, and rill erosion amount were all positively correlated with inflow rates in linear

Table 3

Relative importance (%) of suspension–saltation (SS) and bed load (BL) in sediment during three rill erosion stages.

Soil type	Rill erosion stage	Inflow rate ($\text{L min}^{-1} \text{ m}^{-1}$)									
		8.5		10		11.5		13		14.5	
		SS	BL	SS	BL	SS	BL	SS	BL	SS	BL
<i>UDS</i>	a	91.54	8.46	74.14	25.86	78.12	21.88	66.33	33.67	83.50	16.50
	b	88.67	11.33	72.49	27.51	67.51	32.49	70.90	29.10	74.25	25.75
	c	91.94	8.06	74.33	25.67	79.31	20.69	74.88	25.12	70.39	29.61
<i>UDQ</i>	a	90.48	9.52	88.58	11.42	80.19	19.81	78.56	21.44	73.87	26.13
	b	93.14	6.86	92.14	7.86	78.41	21.59	72.18	27.82	83.38	16.62
	c	84.83	15.17	92.37	7.63	79.65	20.35	76.59	23.41	72.19	27.81

Eroded sediments in three different periods were selected. a: the 2–5 min (rill initiation stage); b: 13–16 min (rill development stage); c: the 24–27 min (rill stable stage). *UDS*: Ultisols derived from shale; *UDQ*: Ultisols derived from quaternary red clay.

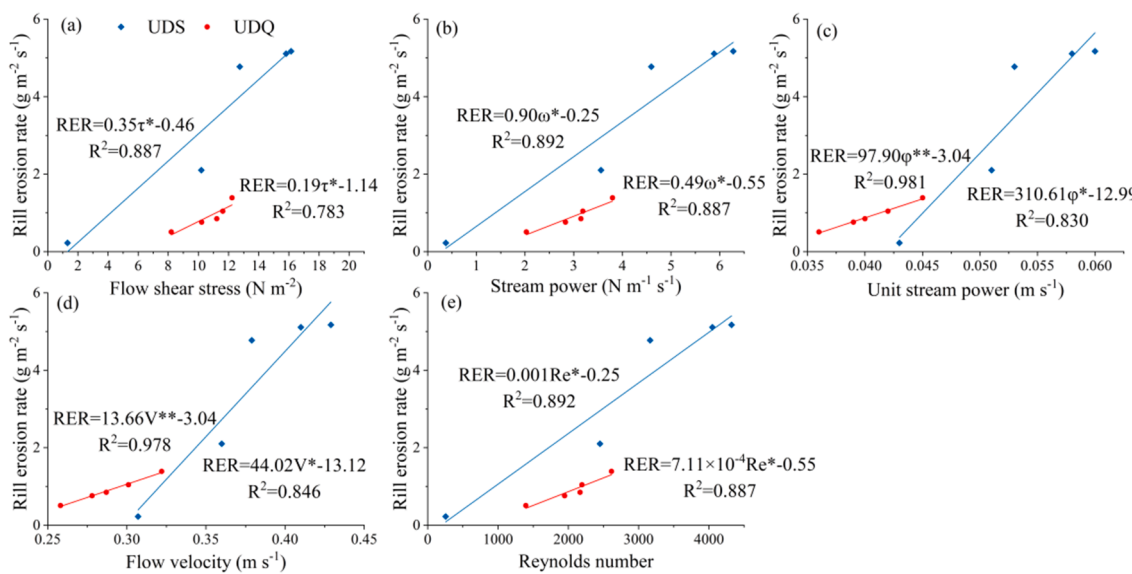


Fig. 11. Fitting Relationships between hydraulic and hydrodynamic parameters and rill erosion rate. RER: rill erosion rate ($\text{g m}^{-2} \text{s}^{-1}$); V: average flow velocity (m s^{-1}); Re: Reynolds Number; Fr: Froude number; f: Darcy–Weisbach resistance coefficient; n: Manning roughness coefficient; τ : flow shear stress (N m^{-2}); ω : stream power ($\text{N m}^{-1} \text{s}^{-1}$); ϕ : unit stream power (m s^{-1}); R^2 : determination coefficients; *: significance at $p < 0.05$ level; **: significance at $p < 0.01$ level.

relationships ($p < 0.05$). The high sand and low clay contents in eroded sediments were closely related to the original soil texture (dominated by clay and silt) and rill flow energy. Stream power and unit stream power were the optimal hydraulic parameters to characterize the rill erosion mechanisms for *UDS* and *UDQ*, respectively. For *UDQ* which had higher clay content and larger bulk density, the smaller fluctuations in the sediment yield processes than *UDS* indicated its more stable rill development processes. In the total eroded sediments of *UDQ*, the higher sand content and lower silt content than that of *UDS* indicated its higher aggregate water stability against slaking. The rill flow of *UDQ* had slower velocity and larger Darcy–Weisbach resistance coefficient than that of *UDS*. For *UDS* which had lower clay and higher sand content, the average sediment yield rate of it was 2.26–4.71 times of *UDQ*, indicating its more unstable soil property and weaker anti-erodibility. The average rill depth of *UDS* was 2.79–6.53 times of *UDQ*, which indicated its more severe downcutting erosion during rill development processes. The rill erodibility parameter of *UDS* was 1.84 times that of *UDQ*. And the critical flow shear stress and stream power of *UDQ* for rill erosion occurring were much higher than that of *UDS*.

The findings allow to better understand the rill erosion mechanisms on red soil slopes, and provide important guidance for preventing the rill erosion of hillslope Ultisols in subtropical regions. As the inflow rate and soil physical property had significant impacts on the erosion and rill development processes on red soil (Ultisols) slopes, the measures taking to weaken the erosive power of slope flow and improve soil quality, such as hedgerow, straw mulching and intercropping system are useful for controlling soil erosion. Further research is needed to better understand the water erosion mechanisms on red soil slopes so that more effective measures can be taken to control slope erosion and prevent rill formation.

Declaration of Competing Interest

The authors declare that they have no known competing financial interests or personal relationships that could have appeared to influence the work reported in this paper.

Acknowledgments

This research was jointly funded by the National Natural Science

Foundation of China (41907061), the Natural Science Foundation of Hubei province, China (2021CFB550), the Research Program from the State Key Laboratory of Soil Erosion and Dryland Farming on the Loess Plateau (A314021402-2005), and the Natural Science Basic Research Program of Shaanxi Province (2021JQ-165).

References

- Asadi, H., Moussavi, A., Ghadiri, H., Rose, C.W., 2011. Flow-driven soil erosion processes and the size selectivity of sediment. *J. Hydrol.* 406 (1), 73–81. <https://doi.org/10.1016/j.jhydrol.2011.06.010>.
- Assouline, S., Ben-Hur, M., 2006. Effects of rainfall intensity and slope gradient on the dynamics of interrill erosion during soil surface sealing. *Catena* 66 (3), 211–220. <https://doi.org/10.1016/j.catena.2006.02.005>.
- Berger, C., Schulze, M., Rieke-Zapp, D., Schlunegger, F., 2010. Rill development and soil erosion: A laboratory study of slope and rainfall intensity. *Earth Surf. Process. Landf.* 35 (12), 1456–1467. <https://doi.org/10.1002/esp.1989>.
- Brecheisen, Zachary S., Richter, Daniel DeB., 2021. Gully-erosion estimation and terrain reconstruction using analyses of microtopographic roughness and LiDAR. *Catena* 202 (7), 105264. <https://doi.org/10.1016/j.catena.2021.105264>.
- Bronick, C.J., Lal, R., 2005. Soil structure and management: a review. *Geoderma* 124 (1–2), 3–22. <https://doi.org/10.1016/j.geoderma.2004.03.005>.
- Bruno, Carmelo, Stefano, Costanza Di, Ferro, Vito, 2008. Field investigation on rilling in the experimental Sparacia area, South Italy. *Earth Surf. Process. Landf.* 33 (2), 263–279. <https://doi.org/10.1002/esp.1544>.
- Brunton, D.A., Bryan, R.B., 2000. Rill network development and sediment budgets. *Earth Surf. Proc. Land.* 25 (7), 783–800.
- Cai, G.Q., Zhu, Y.D., Wang, S.Y., 2004. Research on processes and factors of rill erosion. *Adv. Water Sci.* 15 (1), 12–18 in Chinese.
- Chappell, N.A., Ternan, J.L., Bidin, K., 1999. Correlation of physicochemical properties and sub-erosional landforms with aggregate stability variations in a tropical ultisol disturbed by forestry operations. *Soil Tillage Res.* 50 (1), 55–71. [https://doi.org/10.1016/S0167-1987\(98\)00196-2](https://doi.org/10.1016/S0167-1987(98)00196-2).
- da Silva, Cillas Pollicarto, de Almeida, Brivaldo Gomes, Romero, Ricardo Espíndola, de Alencar, Thiago Leite, Lobato, Marcio Godofredo Rocha, Oliveira, Lucas de Sousa, Souza, Luciano da Silva, Costa, Mirian Cristina Gomes, Mota, Jaedson Cláudio Anunciação, 2020. Cohesive character in Alfisols, Ultisol and Oxisols in northeast of Brazil: Relationship with tensile strength and particle size. *Geoderma Regional* 23, e00341. <https://doi.org/10.1016/j.geodrs.2020.e00341>.
- Defersha, M.B., Melesse, A.M., 2012. Effect of rainfall intensity, slope and antecedent moisture content on sediment concentration and sediment enrichment ratio. *Catena* 90, 47–52. <https://doi.org/10.1016/j.catena.2011.11.002>.
- Di Stefano, C., Nicosia, A., Palmeri, V., Pampalone, V., Ferro, V., 2021. Estimating flow resistance in steep slope rills. *Hydrological Processes* 35 (7), e14296. <https://doi.org/10.1002/hyp.14296>.
- Ding, W., Huang, C., 2017. Effects of soil surface roughness on interrill erosion processes and sediment particle size distribution. *Geomorphology* 295, 801–810. <https://doi.org/10.1016/j.geomorph.2017.08.033>.
- Durnford, Deanna, King, J. Phillip, 1993. Experimental study of processes and particle-size distributions of eroded soil. *J. Irrig. Drain. Eng.* 119 (2), 383–398. [https://doi.org/10.1061/\(ASCE\)0733-9437\(1993\)119:2\(383\)](https://doi.org/10.1061/(ASCE)0733-9437(1993)119:2(383)).

- Fang, Haiyan, Sun, Liying, Tang, Zhenghong, 2015. Effects of rainfall and slope on runoff, soil erosion and rill development: an experimental study using two loess soils. *Hydrol. Process.* 29 (11), 2649–2658. <https://doi.org/10.1002/hyp.10392>.
- Fang, N.F., Wang, L., Shi, Z.H., 2017. Runoff and soil erosion of field plots in a subtropical mountainous region of China. *J. Hydrol.* 552, 387–395. <https://doi.org/10.1016/j.jhydrol.2017.06.048>.
- Foster, G.R., Huggins, L.F., Meyer, L.D., 1984. A laboratory study of rill hydraulics: I. Velocity relationship. *Trans. ASAE* 27 (3), 790–796. [10.13031/2013.32873](https://doi.org/10.13031/2013.32873).
- Gatto, L.W., 2000. Soil freeze-thaw-induced changes to a simulated rill: potential impacts on soil erosion. *Geomorphology* 32 (1), 147–160. [https://doi.org/10.1016/S0169-555X\(99\)00092-6](https://doi.org/10.1016/S0169-555X(99)00092-6).
- Giménez, Rafael, Govers, Gerard, 2002. Flow detachment by concentrated flow on smooth and irregular beds. *Soil Sci. Soc. Am.* 66 (9), 1475–1483. <https://doi.org/10.2136/sssaj2002.1475>.
- Govindaraju, R.S., Kavvas, M.L., 1994. A spectral approach for analyzing the rill structure over hillslopes. Part 2. Application. *J. Hydrol.* 158 (3/4), 349–362. [https://doi.org/10.1016/0022-1694\(94\)90062-0](https://doi.org/10.1016/0022-1694(94)90062-0).
- Govers, G., Giménez, R., Van Oost, K., 2007. Rill erosion: Exploring the relationship between experiments, modelling and field observations. *Earth-Sci. Rev.* 84 (3), 87–102. <https://doi.org/10.1016/j.earscirev.2007.06.001>.
- Guo, Z.L., Ma, M.J., Cai, C.F., Wu, Y.W., 2018. Combined effects of simulated rainfall and overland flow on sediment and solute transport in hillslope erosion. *J. Soils Sedim.* 18 (3), 1120–1132. <https://doi.org/10.1007/s11368-017-1868-0>.
- Hao, H.X., Wang, J.G., Guo, Z.L., Hua, L., 2019. Water erosion processes and dynamic changes of sediment size distribution under the combined effects of rainfall and overland flow. *Catena* 173, 494–504. <https://doi.org/10.1016/j.catena.2018.10.029>.
- He, J.J., Sun, L.Y., Gong, H.L., Cai, Q.G., Jia, L.J., 2016. The characteristics of rill development and their effects on runoff and sediment yield under different slope gradients. *J. Mt. Sci.* 13 (3), 397–404. <https://doi.org/10.1007/s11629-015-3490-1>.
- Imhoff, S., da Silva, A., Pires, Dexter, A., 2002. Factors contributing to the tensile strength and friability of Oxisols. *Soil Sci. Soc. Am. J.* 66 (5), 1656–1661. <https://doi.org/10.2136/sssaj2002.1656>.
- Jafarpour, Atefeh, Sadeghi, Seyed Hamidreza, Zarei Darki, Behrouz, Homaei, Mehdi, 2022. Changes in morphologic, hydraulic, and hydrodynamic properties of rill erosion due to surface inoculation of endemic soil cyanobacteria. *Catena* 208, 105782. <https://doi.org/10.1016/j.catena.2021.105782>.
- Kimaro, D.N., Poesen, J., Msanya, B.M., Deckers, J.A., 2008. Magnitude of soil erosion on the northern slope of the Uluguru Mountains, Tanzania: Interrill and rill erosion. *Catena* 75 (1), 38–44. <https://doi.org/10.1016/j.catena.2008.04.007>.
- Knapen, A., Poesen, J., De Baets, S., 2007. Seasonal variations in soil erosion resistance during concentrated flow for a loess-derived soil under two contrasting tillage practices. *Soil Till. Res.* 94 (2), 425–440. <https://doi.org/10.1016/j.still.2006.09.005>.
- Kou, P.L., Xu, Q., Yunus, A.P., Dong, X.J., Zhong, Y.J., Chen, L.W., Fang, S.A., Luo, X.B., Jin, Z., 2021. Rill development and its change rate: a field experiment under constant rainfall intensity. *Catena* 199 (12), 105112. <https://doi.org/10.1016/j.catena.2020.105112>.
- Luffman, I.E., Nandi, A., Spiegel, T., 2015. Gully morphology, hillslope erosion, and precipitation characteristics in the Appalachian Valley and Ridge province, southeastern USA. *Catena* 133, 221–232. <https://doi.org/10.1016/j.catena.2015.05.015>.
- Luk, S.H., Merz, W., 1992. Use of the salt tracing technique to determine the velocity of overland-flow. *Soil Till. Res.* 5, 289–301.
- Lu, S.G., Malik, Z., Chen, D.P., Wu, C.F., 2014. Porosity and pore size distribution of ultisols and correlations to soil iron oxides. *Catena* 123, 79–87. <https://doi.org/10.1016/j.catena.2014.07.010>.
- Ma, R.M., Li, Z.X., Cai, C.F., Wang, J.G., 2014. The dynamic response of splash erosion to aggregate mechanical breakdown through rainfall simulation events in Ultisols (subtropical China). *Catena* 121 (7), 279–287. <https://doi.org/10.1016/j.catena.2014.05.028>.
- Ma, X.L., Zhang, K.D., Yang, F., Yang, M.Y., Dong, X., 2017. Influencing factor analysis of rill erosion section morphology development on slope and its dynamic characteristic experiment. *Trans. Chin. Soc. Agric. Eng.* 33 (4), 209–216 in Chinese.
- Malam Issa, O., Le Bissonnais, Y., Planchon, O., Favis-Mortlock, D., Silveira, N., Wainwright, J., 2006. Soil detachment and transport on field- and laboratory-scale interrill areas: erosion processes and the size-selectivity of eroded sediment. *Earth Surf. Proc. Land.* 31, 929–939. <https://doi.org/10.1002/esp.1303>.
- Mancilla, G.A., Chen, S., McCool, D.K., 2005. Rill density prediction and flow velocity distribution on agricultural areas in the Pacific Northwest. *Soil Till. Res.* 84 (1), 54–66. <https://doi.org/10.1016/j.still.2004.10.002>.
- Meyer, L.D., Line, D.E., Harmon, W.C., 1992. Size characteristics of sediment from agricultural soils. *J. Soil Water Conserv.* 47 (1), 107–111.
- Miao, C.Y., Ni, J.R., Borthwick, A.G.L., 2010. Recent changes in water discharge and sediment load of the Yellow River basin, China. *Prog. Phys. Geogr.* 34 (4), 541–561. <https://doi.org/10.1177/0309133310369434>.
- Morgan, R.P.C., Quinton, J.N., Smith, R.E., Govers, G., Poesen, J.W.A., Auerswald, K., Chisci, G., Torri, D., Styczen, M. E., 1998. The European Soil Erosion Model (EUROSEM): A dynamic approach for predicting sediment transport from fields and small catchments. *Earth Surf. Process. Landf.* 23 (6), 527–544. [10.1002/\(SICI\)1096-9837\(199806\)23:6<527::AID-ESP868>3.0.CO;2-5](https://doi.org/10.1002/(SICI)1096-9837(199806)23:6<527::AID-ESP868>3.0.CO;2-5).
- Muhs, D.R., Bettis, E.A., Been, J., McGeehin, J.P., 2001. Impact of climate and Parent Material on Chemical Weathering in Loess-derived Soils of the Mississippi River Valley. *Soil Sci. Soc. Am. J.* 65 (6), 1761–1777. [10.2136/sssaj2001.1761](https://doi.org/10.2136/sssaj2001.1761).
- Nearing, M.A., G.R. Foster, L.J. Lane, and S.C. Finkner. 1989. A process-based soil erosion model for USDA-Water Erosion Prediction Project technology. *Trans. ASAE* 32:1587–1593. [10.13031/2013.31195](https://doi.org/10.13031/2013.31195).
- Nearing, M.A., Simanton, J.R., Norton, L.D., Bulygin, S.J., Stone, J., 1999. Soil erosion by surface water flow on a stony, semiarid hillslope. *Earth Surf. Process. Landf.* 24 (8), 677–686. [10.1002/\(SICI\)1096-9837\(199908\)24:8<677::AID-ESP981>3.0.CO;2-1](https://doi.org/10.1002/(SICI)1096-9837(199908)24:8<677::AID-ESP981>3.0.CO;2-1).
- Niu, Yaobin, Gao, Zhaoliang, Li, Yonghong, Lou, Yongcui, Zhang, Shuai, Zhang, Letao, Du, Jie, Zhang, Xiang, Luo, Ke, 2020. Characteristics of rill erosion in spoil heaps under simulated inflow: a field runoff plot experiment. *Soil Tillage Res.* 202, 104655. <https://doi.org/10.1016/j.still.2020.104655>.
- Ou, Xiaojing, Hu, Yaxian, Li, Xianwen, Guo, Shengli, Liu, Baoyuan, 2021. Advancements and challenges in rill formation, morphology, measurement, and modeling. *Catena* 196, 104932. <https://doi.org/10.1016/j.catena.2020.104932>.
- Rawlins, B.G., Webster, R., Lister, T.R., 2003. The influence of parent material on topsoil geochemistry in eastern England. *Earth Surf. Process. Landf.* 28 (13), 1389–1409. [10.1002/esp.507](https://doi.org/10.1002/esp.507).
- Rejman, Jerzy, Brodowski, Ryszard, 2005. Rill characteristics and sediment transport as a function of slope length during a storm event on loess soil. *Earth Surf. Process. Landforms* 30 (2), 231–239. <https://doi.org/10.1002/esp.1177>.
- Peng, Wenying, Zhang, Zhuodong, Zhang, Keli, 2015. Hydrodynamic characteristics of rill flow on steep slopes. *Hydrol. Process.* 29 (17), 3677–3686. <https://doi.org/10.1002/hyp.10461>.
- Peng, X., Zhu, Q.H., Xie, Z.B., Darboux, F., Holden, N.M., 2016. The impact of manure, straw and biochar amendments on aggregation and erosion in a hillslope Ultisol. *Catena* 138, 30–37. <https://doi.org/10.1016/j.catena.2015.11.008>.
- Rodrigo-Comino, Jesús, Novara, Agata, Gyasi-Agyei, Yeboah, Terol, Enric, Cerdà, Artemi, 2018. Effects of parent material on soil erosion within Mediterranean new vineyard plantations. *Eng. Geol.* 246, 255–261. <https://doi.org/10.1016/j.enggeo.2018.10.006>.
- Saygin, S.D., Erpul, G., 2019. Modeling aggregate size distribution of eroded sediment resulting from rain-splash and raindrop impacted flow processes. *Int. J. Sediment Res.* 34 (2), 166–177. <https://doi.org/10.1016/j.ijscrc.2018.10.004>.
- Shen, H.O., Zheng, F.L., Wen, L.L., Lu, J., Jiang, Y.L., 2015. An experimental study of rill erosion and morphology. *Geomorphology* 231, 193–201. <https://doi.org/10.1016/j.geomorph.2014.11.029>.
- Shen, H.O., Zheng, F.L., Wen, L.L., Han, Y., Hu, W., 2016. Impacts of rainfall intensity and slope gradient on rill erosion processes at loessial hillslope. *Soil Till. Res.* 155, 429–436. <https://doi.org/10.1016/j.still.2015.09.011>.
- Shi, Z.H., Yan, F.L., Li, L., Li, Z.X., Cai, C.F., 2010. Interrill erosion from disturbed and undisturbed samples in relation to topsoil aggregate stability in red soils from subtropical China. *Catena* 81 (3), 240–248. <https://doi.org/10.1016/j.catena.2010.04.007>.
- Shi, Z.H., Fang, N.F., Wu, F.Z., Wang, L., Yue, B.J., Wu, G.L., 2012. Soil erosion processes and sediment sorting associated with transport mechanisms on steep slopes. *J. Hydrol.* 454, 123–130. <https://doi.org/10.1016/j.jhydrol.2012.06.004>.
- Shi, Z.H., Yue, B.J., Wang, L., Fang, N.F., Wang, D., Wu, F.Z., 2013. Effects of mulch cover rate on interrill erosion processes and the size selectivity of eroded sediment on steep slopes. *Soil Sci. Soc. Am. J.* 77 (1), 257–267. <https://doi.org/10.2136/sssaj2012.0273>.
- Shi, Z.L., Wen, A.B., Walling, D.E., Wang, Y.Y., Chen, J.C., 2017. Exploring particle size selectivity effects during erosion of purplesoils in Chongqing municipality, China. *Journal of Soils and Sediments* 17 (4), 1191–1196. <https://doi.org/10.1007/s11368-016-1619-7>.
- Stefano, C.D., Ferro, V., Pampalone, V., Sanzone, F., 2013. Field investigation of rill and ephemeral gully erosion in the Sparacia experimental area, South Italy. *Catena* 101, 226–234. <https://doi.org/10.1016/j.catena.2012.10.012>.
- Tang, S.S., Gao, H.D., Li, Z.B., Ren, Z.P., Zhang, H., Su, Y., Zhi, Z., 2017. Characteristics of particle separation of erosion sediment in slop surface covered with sand. *Trans. CSAE* 33 (2), 125–130 in Chinese.
- Tian, P., Pan, C., Xu, X., Wu, T., Yang, T., Zhang, L., 2020. A field investigation on rill development and flow hydrodynamics under different upslope inflow and slope gradient conditions. *Hydrology Research* 51 (5), 1201–1220. <https://doi.org/10.2166/nh.2020.168>.
- Tian, P., Xu, X.Y., Pan, C.Z., Hsu, K.L., Yang, T.T., 2017. Impacts of rainfall and inflow on rill formation and erosion processes on steep hillslopes. *J. Hydrol.* 548, 24–39. <https://doi.org/10.1016/j.jhydrol.2017.02.051>.
- Tian, P., Zhu, Z., Yue, Q., He, Y., Zhang, Z., Hao, F., Guo, W., Chen, L., Liu, M., 2021. Soil Erosion Assessment by RUSLE with Improved P Factor and its validation: Case Study on Mountainous and Hilly Areas of Hubei Province, China. *International Soil and Water Conservation Research* 9, 433–444. <https://doi.org/10.1016/j.iswcr.2021.04.007>.
- Vinci, A., Brigante, R., Todisco, F., Mannocchi, F., Radicioni, F., 2015. Measuring rill erosion by laser scanning. *Catena* 124, 97–108. <https://doi.org/10.1016/j.catena.2014.09.003>.
- Wang, Jun-guang, Li, Zhao-xia, Cai, Chong-fa, Yang, Wei, Ma, Ren-ming, Zhang, Guo-biao, 2012. Predicting physical equations of soil detachment by simulated concentrated flow in Ultisols (subtropical China). *Earth Surf. Process. Land.* 37 (6), 633–641. <https://doi.org/10.1002/esp.3195>.
- Wang, J.G., Yang, W., Yu, B., Li, Z.X., Cai, C.F., Ma, R.M., 2016. Estimating the influence of related soil properties on macro- and micro-aggregate stability in ultisols of southcentral China. *Catena* 137, 545–553. <https://doi.org/10.1016/j.catena.2015.11.001>.
- Wang, L., Shi, Z.H., Wang, J., Fang, N.F., Wu, G.L., Zhang, H.Y., 2014. Rainfall kinetic energy controlling erosion processes and sediment sorting on steep hillslopes: a case study of clay loam soil from the Loess Plateau, China. *J. Hydrol.* 512, 168–176. <https://doi.org/10.1016/j.jhydrol.2014.02.066>.

- Wang, N., Ding, L., Liu, G.C., Deng, Q.C., Liu, H., Wang, J., Lv, W., Luo, J., Du, Z.Y., Zhang, B., 2019. Variation of rill cross-sections with gravel and aggregating soil in the Dry-Hot Valley (SW China). *Modeling Earth Systems and Environment* 5 (4), 1239–1252. <https://doi.org/10.1007/s40808-019-00632-9>.
- Wan, Y.S., El-Swaify, S.A., 1997. Flow-induced transport and enrichment of erosional sediment from a well-aggregated and uniformly-textured Oxisol. *Geoderma* 75 (3), 251–265. [https://doi.org/10.1016/S0016-7061\(96\)00093-6](https://doi.org/10.1016/S0016-7061(96)00093-6).
- Wei, Y., Wu, X., Cai, C., 2015. Splash erosion of clay-sand mixtures and its relationship with soil physical properties: The effects of particle size distribution on soil structure. *Catena* 135, 254–262. <https://doi.org/10.1016/j.catena.2015.08.003>.
- Wei, Yujie, Wu, Xinliang, Xia, Jinwen, Shen, Xue, Cai, Chongfa, Reigosa, Manuel, 2016. Variation of soil aggregation along the weathering gradient: comparison of grain size distribution under different disruptive forces. *PLoS One* 11 (8), e0160960. <https://doi.org/10.1371/journal.pone.0160960>.
- Wirtz, S., Seeger, M., Ries, J.B., 2012. Field experiments for understanding and quantification of rill erosion processes. *Catena* 91, 21–34. <https://doi.org/10.1016/j.catena.2010.12.002>.
- Wirtz, Stefan, Seeger, Manuel, Zell, Andreas, Wagner, Christian, Wagner, Jean-Frank, Ries, Johannes B., Magar, Vanesa, 2013. Applicability of different hydraulic parameters to describe soil detachment in eroding rills. *PLoS One* 8 (5), e64861. <https://doi.org/10.1371/journal.pone.0064861>.
- Wu, X.L., Wei, Y.J., Li, Z.X., Cai, C.F., Yang, W., 2014. Composition of sediments of erosion from different red soil slopes in subtropical area. *Acta Pedologica Sinica* 51 (6), 1223–1233 in Chinese.
- Wu, X.L., Wei, Y.J., Wang, J.G., Xia, J.W., Cai, C.F., Wu, L.L., Fu, Z.Y., Wei, Z.Y., 2017. Effects of erosion degree and rainfall intensity on erosion processes for Ultisols derived from quaternary red clay. *Agric. Ecosyst. Environ.* 249, 226–236. <https://doi.org/10.1016/j.agee.2017.08.023>.
- Wu, X.L., Wei, Y.J., Wang, J.G., Xia, J.W., Cai, C.F., Wei, Z.Y., 2018. Effects of soil type and rainfall intensity on sheet erosion processes and sediment characteristics along the climatic gradient in central-south China. *Sci. Total Environ.* 621, 54–66. <https://doi.org/10.1016/j.scitotenv.2017.11.202>.
- Wu, Xinliang, Wei, Yujie, Cai, Chongfa, Yuan, Zaijian, Li, Dingqiang, Liao, Yishan, Deng, Yusong, 2021. Quantifying the contribution of phyllosilicate mineralogy to aggregate stability in the East Asian monsoon region. *Geoderma* 393, 115036. <https://doi.org/10.1016/j.geoderma.2021.115036>.
- Xiao, Hai, Liu, Gang, Liu, Puling, Zheng, Fenli, Zhang, Jiaqiong, Hu, Feinan, 2017. Developing equations to explore relationships between aggregate stability and erodibility in Ultisols of subtropical China. *Catena* 157, 279–285. <https://doi.org/10.1016/j.catena.2017.05.032>.
- Yan, F., Shi, Z., Li, Z., Cai, C., 2008. Estimating interrill soil erosion from aggregate stability of Ultisols in subtropical China. *Soil Tillage Res.* 100 (1–2), 34–41. <https://doi.org/10.1016/j.still.2008.04.006>.
- Yan, Feng-Ling, SHI, Zhi-Hua, CAI, Chong-Fa, LI, Zhao-Xia, 2010. Wetting rate and clay content effects on interrill erosion in Ultisols of southeastern China. *Pedosphere* 20 (1), 129–136. [https://doi.org/10.1016/S1002-0160\(09\)60292-7](https://doi.org/10.1016/S1002-0160(09)60292-7).
- Yang, W., Zhang, Q., Li, Z.X., Zhang, L.C., Cai, C.F., 2016. Estimating sediment characters of several typical red soils by simulated rainfall. *Resources and Environment in the Yangtze Basin* 25 (3), 439–444 in Chinese.
- Young, R.A., 1980. Characteristics of eroded sediment. *Trans. ASAE* 23 (1139–1142), 1146.
- YU, Dong-Sheng, SHI, Xue-Zheng, WEINDORF, D.C., 2006. Relationships between permeability and erodibility of cultivated Acrisols and Cambisols in subtropical China. *Pedosphere* 16 (3), 304–311. [https://doi.org/10.1016/S1002-0160\(06\)60056-8](https://doi.org/10.1016/S1002-0160(06)60056-8).
- Zhang, B., Zhang, T.L., Zhao, Q.G., 1996. Soil erosion of various farming systems in subtropical China. *Pedosphere* 6 (3), 225–233.
- Zhang, B., Yang, Y.S., Zepp, H., 2004. Effect of vegetation restoration on soil and water erosion and nutrient losses of a severely eroded clayey Plinthudult in southeastern China. *Catena* 57 (1), 77–90. <https://doi.org/10.1016/j.catena.2003.07.001>.
- Zhang, G.H., Liu, B.Y., Liu, G.B., He, X.W., Nearing, M.A., 2003. Detachment of Undisturbed Soil by Shallow Flow. *Soil Sci. Soc. Am. J.* 67 (3), 713–719. <https://doi.org/10.2136/sssaj2003.7130>.
- Zhang, K.L., Zhang, Z.M., 2000. Erosion and sediment delivery in rills on steep loess slope. *Prog. Nat. Sci.* 10, 794–797.
- Zhang, L.T., Gao, Z.L., Yang, S.W., Li, Y.H., Tian, H.W., 2015. Dynamic processes of soil erosion by runoff on engineered landforms derived from expressway construction: a case study of typical steep spoil heap. *Catena* 128, 108–121. <https://doi.org/10.1016/j.catena.2015.01.020>.
- Zhang, P., Tang, H.W., Yao, W.Y., Zhang, N., Lv, X.Z., 2016. Experimental investigation of morphological characteristics of rill evolution on loess slope. *Catena* 137, 536–544. <https://doi.org/10.1016/j.catena.2015.10.025>.
- Zhao, C.H., Gao, J.E., 2016. Cross-section characteristics and hydraulic geometry of different erosion gullies on slopes. *Adv. Water Sci.* 27 (1), 22–30 (In Chinese). <https://doi.org/10.14042/j.cnki.32.1309.2016.01.001>.
- Zhao, Q.H., Li, D.Q., Zhuo, M.N., Guo, T.L., Liao, Y.S., Xie, Z.Y., 2015. Effects of rainfall intensity and slope gradient on erosion characteristics of the red soil slope. *Stoch. Environ. Res. Risk Assess.* 29 (2), 609–621. <https://doi.org/10.1007/s00477-014-0896-1>.